scientific reports

Check for updates

OPEN

Selective targeting of genes regulated by zinc finger proteins in endometriosis and endometrioid adenocarcinoma by zinc niflumato complex with neocuproine

Ivana Špaková[1], Lukáš Smolko[1], Gabriela Sabolová[1], Zuzana Badovská[1], Katarína Kalinová[2], Corina Madreiter-Sokolowski[2], Wolfgang F. Graier[2], Mária Mareková[1], Janka Vašková[1] & Miroslava Rabajdová[1]✉

Inadequate angiogenesis of endometriotic implants stimulated by the inflammatory microenvironment in the uterine region leads to the development of gynecological diseases, which significantly reduce the fertility and vitality of young women. Angiogenic processes are controlled by factors whose activities are regulated at the gene level by reactive oxygen species (ROS), hypoxia-induced factors (HIFs), and zinc-finger proteins (ZnFs) or posttranscriptionally via non-coding RNAs. The cooperation of these factors is responsible for the manifestation of pathological stimuli in the form of endometriosis of the body of the uterus, ovaries, or peritoneum, from which endometrioid carcinoma can develop. Molecules that can control gene expression by their intercalation to target DNA sequence, such as [Zn(neo)(nif)$_2$], could prevent the hyperactivation of pro-angiogenic pathways (decrease HIF-1α, VEGF-A, TGF-β1, COX2, and ANG2/ANG1), reduce the formation of ROS, and reduce the risk of uterine neoplasticity. The NSAID-metal complex [Zn(neo)(nif)$_2$] shows an ability to intercalate into ZNF3-7 target DNA sequence at a higher rate, which could explain its effect on genes regulated by this transcription factor. In addition, [Zn(neo)(nif)$_2$] affects ROS production and Ca^{2+} level, possibly pointing to mitochondrial dysfunction as a potential cause for the described apoptosis.

Keywords Endometriosis, Endometrioid adenocarcinoma, [Zn(neo)(nif)$_2$], Angiogenesis, Ca^{2+}, ROS

Pathologies in the pelvis primarily arise from the attachment and growth of endometriotic implants in a non-physiological environment – outside the uterine cavity. This process is altered by uncontrolled angiogenesis, which bypasses the physiological immune response and elevates hypoxia-inflammatory conditions, driving the transition of eutopic endometrium to ectopic endometriosis and its potential malignant transformation. The transition of endometriosis to a malignant state is regulated by molecular mechanisms with key factors such as HIF-1α (hypoxia-inducible factor 1α), COX2 (cyclooxygenase 2), VEGF-A (vascular endothelial growth factor A), zinc-fingers (ZNFs)[1], Nrf2-ARE (nuclear factor erythroid 2-related factor 2 – antioxidant response element)[2] and microRNAs (miRs)[3].

All these transcription factors (TFs) are necessary for the physiological regulation of uterine lining renewal during the menstrual cycle and embryo implantation. For instance, hypoxia induced by a physiological decrease in progesterone (P4) levels increases the activity of the transcription factor HIF-1α together with COX2, which regulates the synthesis of prostaglandins (PGs)[4]. The rapid transition to severe hypoxia due to the interruption of blood supply in the uterine endothelium by vessel coiling[5] activates apoptotic signals, allowing immune cells to remove epithelial cells during menstruation. Inadequate, prolonged local hypoxia significantly stimulates pathological angiogenesis[6] by suppressing apoptosis while promoting an inflammatory microenvironment[7]. Hypoxia-accelerated implantation of viable endometriotic cells occurs through the production of pro-angiogenic

[1]Department of Medical and Clinical Biochemistry, P. J. Šafárik University in Košice, Trieda SNP 1, 04011 Košice, Slovakia. [2]Gottfried Schatz Research Center for Cell Signaling, Metabolism and Aging Molecular Biology and Biohemistry, Medical University of Graz, Neue Stiftingtalstrasse 6/4, T8010 Graz, Austria. ✉email: miroslava.rabajdova@upjs.sk

factors (VEGF, PGF, TGF, Ang-1)[8], which are released into the surrounding tissue and bind to capillaries and arterioles, promoting the formation of new blood vessels[9]. This hypoxia-mediated angiogenesis is also targeted by miR-206[10,11], -376a[12], and let-7c[13], which acts as an inhibitor of angiogenesis, whereas miR-133b or miR-23a serve as promoters of angiogenesis[12].

MicroRNAs can further regulate the expression of ZNFs, as they contain many seed-matched sequences predominantly localized to the ZNF regions coding the C2H2 domain[14]. The absence of the specific ZNF3 domain suppresses auto-ADP-ribosylation of PARP[15], which is involved in DNA repair, angiogenesis, and chemoresistance of gynecological pathologies[16]. ZNF3 selectively inhibits PARP1 (poly(ADP-ribose) polymerase 1), which could serve as a potential therapeutic target for tumor treatment[17]. In endometriosis, elevated reactive oxygen species (ROS) and mitochondrial dysfunction cause DNA strand breaks and activate DNA repair via PARP. Hyperactivation of PARP by ROS leads to depletion of NAD^+ and ATP and can disrupt calcium homeostasis (increasing intracellular Ca^{2+} levels), exacerbating cellular stress and ultimately leading to cell death[18].

The Nrf2 plays a pivotal role in cellular defense against oxidative stress by regulating antioxidant response elements[19] and has been linked to endoplasmic reticulum (ER) oxidative protein folding and calcium homeostasis[20]. Impaired ER redox signaling can decrease Nrf2 nuclear translocation, resulting in ER calcium overload and increased calcium-dependent cell secretion[20]. In endometriosis, Nrf2 activity is often compromised, resulting in increased oxidative stress and mitochondrial dysfunction[21].

The Nrf2-ARE pathway directly affects neoangiogenesis through the ANG2/ANG1 axis. Nrf2 activation induces antioxidant enzymes (GPx, SOD) that lower reactive oxygen species (ROS) levels, thereby modulating inflammation and ensuring vascular stability[2]. In both physiological and pathological conditions, such as endometriosis and endometrial carcinoma, the balance between angiopoietins ANG1 and ANG2 is essential for vascular homeostasis. ANG1 stabilizes blood vessels via the Tie2 receptor, while ANG2 antagonizes this effect, promoting vascular remodeling and increased permeability, particularly in the presence of VEGF[22,23].

Oxidative stress and inflammatory cytokines can upset this balance by increasing ANG2 expression, leading to abnormal angiogenesis in gynecological disorders. The Nrf2-ARE pathway, through antioxidant responses, helps counteract these effects by reducing ROS levels and restoring the ANG1/ANG2 ratio, promoting normal vascular function[24].

Evidence suggests that interactions between the Nrf2-ARE pathway and the ANG2/ANG1 axis influence endometrial lesion progression by regulating oxidative stress and inflammation. Prolonged hypoxia may trigger persistent Nrf2 activation, contributing to vascular dysfunction and increased permeability. Zinc-finger proteins (ZnFs) have been identified as potential regulators of the Nrf2-ARE pathway and angiopoietin expression, offering new therapeutic insights. ZnFs maintain redox balance and transcriptional regulation of genes related to endometriotic cell survival and apoptosis resistance[25]. In endometriosis and endometrial carcinoma, dysregulated ZnFs may impair Nrf2 function, exacerbating oxidative stress and promoting pathological angiogenesis via the ANG1/ANG2 axis[26].

Furthermore, ZNFs regulate the activity of tumor growth factor β (TGFβ), which contributes to TIEG overexpression and induces apoptosis[27]. Upregulation of ZNFs is associated with apoptosis resistance through regulating apoptotic genes such as BAX, Bcl-2, and Caspase-3 via ROS-induced oxidative damage[28]. Additionally, ZNFs initiate an inflammatory response, support the implantation and survival of endometriotic lesions on the peritoneal surface, and contribute to the worsening course and development of endometriosis[29].

The integrity of the newly formed vascular system is further regulated by ANG-1 (angiopoietin 1) and ANG-2 (angiopoietin 2), which may interact in the progression of endometriosis and represent potential therapeutic targets for non-steroidal anti-inflammatory drugs (NSAIDs) that influence angiopoietin expression of[30,31]. Suppression of the inflammatory mediator COX2 by NSAIDs poses a challenge in treating chronic inflammatory diseases, as prolonged use of NSAIDs has been shown to increase oxidative stress and disrupt the sensitive antioxidant status of patients[32]. Metal complexes with NSAIDs represent an innovative approach to treating inflammatory diseases, as their effect is not limited to COX2 inhibition but also involves interaction with nucleic acids and direct modulation of the enzyme activity, such as MMPs[33].

Our previous studies demonstrated the potential therapeutic effects of NSAID-biometal complex [Zn(neo)$(nif)_2$] (neo = 2,9-dimethyl-1,10-phenathroline; nif = 2-[3-(trifluoromethyl)anilino]nicotinato), as it exhibited higher cytotoxicity on cells with high inflammatory metabolism[33]. Continuing our investigation of the mechanism of action of this complex, we analyzed the expression of targets involved in angiogenesis activated by hypoxia-inflammatory stimuli.

Results

DNA intercalation

Our previous DNA binding studies performed on samples isolated from endometriotic 12Z and control HME1 cell lines indicated the binding specificity of [Zn(neo)$(nif)_2$][33]. To further investigate the binding specificity of the studied complex, short double-stranded DNA (dsDNA) oligonucleotide sequences were selected for the standard competitive fluorescence binding studies with ethidium bromide. The selected sequences were CCCTC-binding factor zinc-finger protein 3 (ZnF3-7) (5'-TAGCGCCCCCTGCTGGC-3'/3'-ATCGCGGGGGA CGACCG-5') and CCAAT/enhancer-binding proteins (C/EBP) (5'-ATTGCGCAAT-3'/3'-TAACGCGTTA-5'). Both sequences are located in the regulatory regions of their respective genes and are recognized by transcription factors during transcription.

Experimental results showed that the studied complex displaces ethidium bromide and binds to both sequences via intercalation, as indicated by quenching of fluorescence in the DNA-EB complex (Figure S1). A more thorough evaluation of the results revealed a higher affinity of the complex to the ZnF3-7 sequence ($K_{SV} = 2.17(2) \times 10^5\ M^{-1}$) in comparison with the EBP sequence ($K_{SV} = 1.10(3) \times 10^5\ M^{-1}$) (Fig. 1).

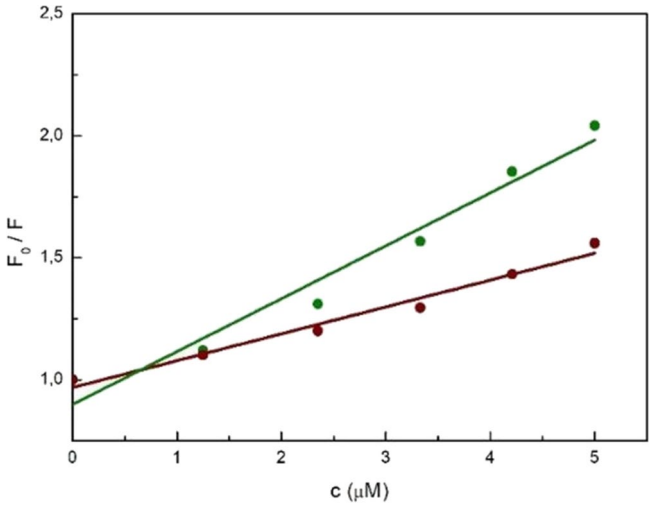

Fig. 1. Comparison of fitted Stern–Volmer plots from competitive binding studies with EB for ZnF3-7 (linear fit 95.8%) (green) and EBP (linear fit 98.4%) (red) dsDNA sequences.

HME1	VEGF-A (P value, significance)	TGF-β1 (P value, significance)	ANG1 (P value, significance)	ANG2 (P value, significance)
control vs. cisPt	0.4763 (ns) ↓	< 0.0001 (***) ↓	0.0002 (***) ↑	0.1982 (ns) ↓
control vs. [Zn(neo)(nif)$_2$]	0.0472 (*) ↓	< 0.0001 (***) ↓	0.0028 (**) ↑	0.1677 (ns) ↓
cisPt vs. [Zn(neo)(nif)$_2$]	0.4306 (ns) ↓	0.9983 (ns) ↑	0.3207 (ns) ↓	0.0337 (*) ↓
12Z				
control vs. cisPt	< 0.0001 (***) ↑	< 0.0001 (***) ↑	0.0056 (**) ↑	0.3062 (ns) ↑
control vs. [Zn(neo)(nif)$_2$]	0.9430 (ns) ↑	0.9516 (ns) ↑	0.0377 (*) ↑	0.0235 (*) ↑
cisPt vs. [Zn(neo)(nif)$_2$]	< 0.0001 (***) ↓	< 0,0001 (***) ↓	0.0088 (**) ↓	0.8098 (ns) ↑
A2780				
control vs. cisPt	0.9940 (ns) ↑	0.7830 (ns) ↑	0.3315 (ns) ↓	0.6487 (ns) ↑
control vs. [Zn(neo)(nif)$_2$]	0.9858 (ns) ↑	0.8925 (ns) ↑	0.8926 (ns) ↑	0.3668 (ns) ↓
cisPt vs. [Zn(neo)(nif)$_2$]	0.9982 (ns) ↓	0.9754 (ns) ↓	0.4056 (ns) ↑	0.2783 (ns) ↓

Table 1. Significance values of VEGF-A, TGF-β1, ANG1, and ANG2 (n = 6) under three tested conditions: control (untreated spheroid cells), cisPt (spheroid cells treated with 10 μM cis-platin), [Zn(neo)(nif)$_2$] (spheroid cells treated with 10 μM [Zn(neo)(nif)$_2$]) across three experimental 3D models.

Angiogenic, inflammatory, antioxidant, and apoptotic gene expression

We determined the relative gene expression of angiogenic factors (VEGF-A, TGF-β1, ANG1, ANG2) (Table 1) as we hypothesize that the [Zn(neo)(nif)$_2$] complex preferentially binds to a ZnF-like sequence, such as ZNF3-7 or other ZNFs. The intercalation of [Zn(neo)(nif)$_2$] into DNA can potentially influence the activity of angiogenic transcription factors. We proved this hypothesis by analyzing the expression of genes that regulate vascular formation in a spheroid model of HME1, 12Z, and A2780 cells.

A non-significant increase in the ANG2/ANG1 gene expression ratio was observed in HME1 cells treated with [Zn(neo)(nif)$_2$] ($P = 0.9812$), as well as in HME1 treated with cisPt ($P = 0.7468$). In the 12Z model, a significant elevation of ANG2/ANG1 ratio was found in the cells treated with cisPt ($P < 0.0001$), as well as in those treated with [Zn(neo)(nif)$_2$] ($P < 0.0001$), compared to untreated control 12Z 3D model cells (Fig. 2A). To compare the efficiency of our compound with standard treatment (cisPt), the ANG2/ANG1 ratio showed a non-significant increase in A2780 cells with cisPt ($P = 0.1243$). In contrast, a significant increase in the ANG2/ANG1 ratio was observed in A2780 cells treated with [Zn(neo)(nif)$_2$] ($P < 0.0001$) (Fig. 2A).

Next, we analyzed the VEGF-A/TGF-β1 ratio as an indicator of angiogenic activity in the samples. Our experiments revealed a significant change in the spheroid cell model of HME1 under tested conditions. In the HME1 model treated with cisPt, a significant increase in the VEGF-A/TGF-β1 ratio was observed ($P < 0.0001$), as well as in the HME1 model treated with [Zn(neo)(nif)$_2$] ($P < 0.0001$). In 12Z cells treated with cisPt, a significant increase in the VEGF-A/TGF-β1 ratio was found ($P = 0.0019$), whereas a non-significant change was observed in the 12Z model treated with [Zn(neo)(nif)$_2$]. In A2780 cells, treatment with both cisPt and [Zn(neo)(nif)$_2$] resulted in significant increases in the VEGF-A/TGF-β1 ratio ($P = 0.0044$ and $P < 0.0001$, respectively) (Fig. 2B).

We analyzed the relative gene expression of angiogenic factors (VEGF-A, TGF-b1, ANG1, ANG2), predicting that the studied complex preferentially binds to a ZnF-like sequence. Although significant changes

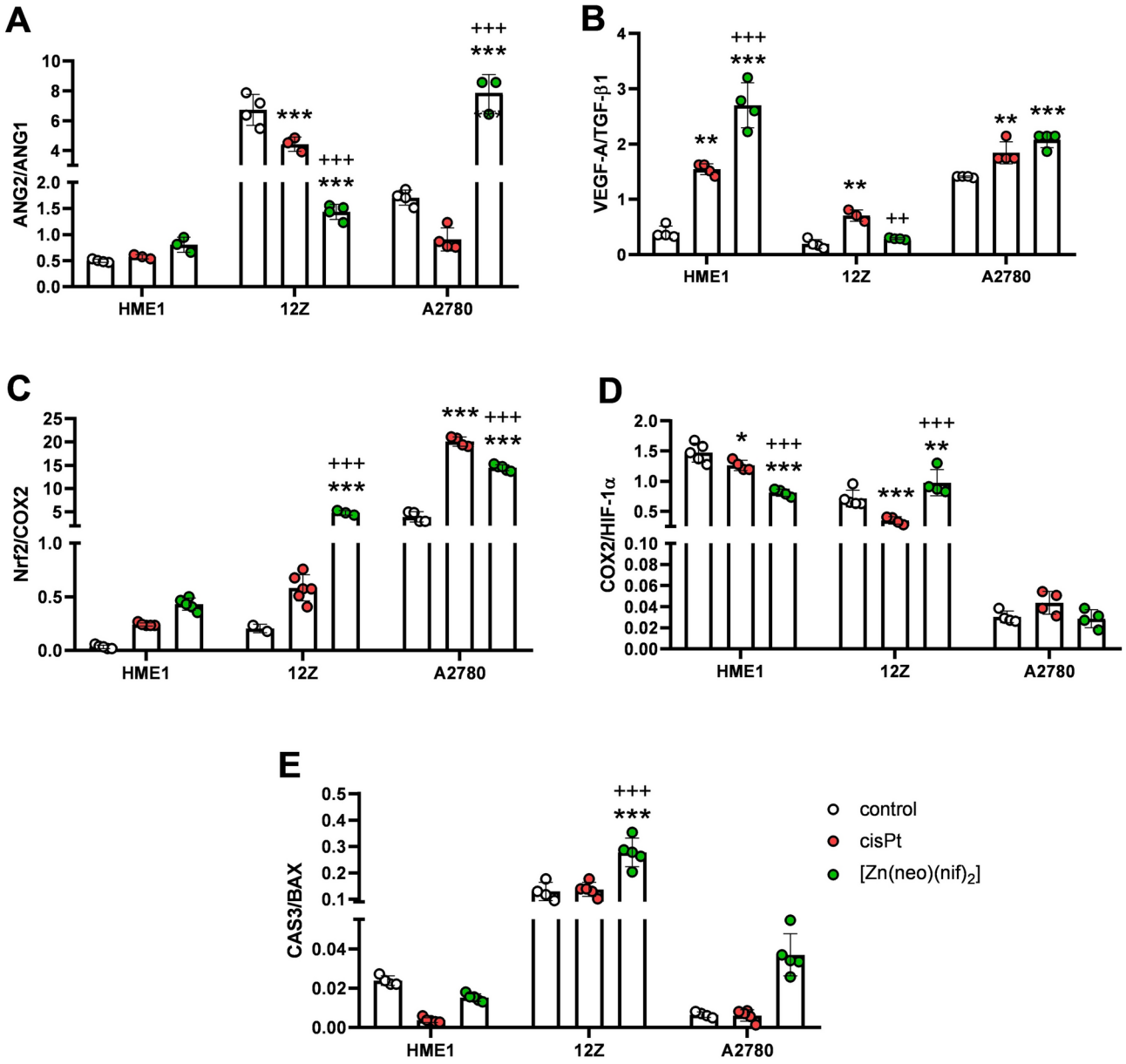

in the individual expression levels of the calculated ratios were observed in specific groups (Table 1), their gene expression did not reach significance across all conditions.

To evaluate the effects of our compound on inflammation and antioxidant activity, the Nrf2/COX2 gene expression showed a non-significant increase in the HME1 model under both conditions: cisPt ($P = 0.8172$) and [Zn(neo)$(nif)_2$] ($P = 0.4868$). In 12Z cells treated with cisPt showed non-significant change ($P = 0.6750$), whereas a significant elevation of Nrf2/COX2 ratio was observed in the 12Z model treated with [Zn(neo)$(nif)_2$] ($P < 0.0001$) (Fig. 2C). In the A2780 model, the Nrf2/COX2 ratio significantly increased under both treated conditions ($P < 0.0001$).

Furthermore, the COX2/HIF-1α ratio was analyzed to evaluate another aspect of the inflammatory impact of our compound. A significant increase in the COX2/HIF-1α gene expression ratio was observed in HME1 cells treated with both cisPt and [Zn(neo)$(nif)_2$] ($P < 0.0001$). The change in the COX2/HIF-1α ratio was also significant in 12Z cells treated with cisPt ($P = 0.0001$) and [Zn(neo)$(nif)_2$] ($P = 0.0044$). In contrast, the change in the COX2/HIF-1α ratio in A2780 cells treated with cisPt ($P = 0.9844$), as well as in those treated with [Zn(neo)$(nif)_2$] ($P = 0.9998$), was non-significant (Fig. 2D).

To evaluate the effect of our test compound on apoptosis-associated gene expression, we selected CAS3 and BAX. A non-significant decrease in the CAS3/BAX gene expression ratio was observed in HME1 cells treated with cisPt ($P = 0.4299$) and in the HME1 model treated with [Zn(neo)$(nif)_2$] ($P = 0.8530$) (Fig. 2E). Similarly, a decrease in the CAS3/BAX ratio was noted in 12Z cells treated with cisPt ($P = 0.8766$), while a significant reduction was observed in the 12Z model treated with [Zn(neo)$(nif)_2$] ($P < 0.0001$). In the A2780 model, the CAS3/BAX ratio remained non-significantly changed under both treatment conditions (cisPt $P = 0.9997$; [Zn(neo)$(nif)_2$] $P = 0.1528$).

◀**Fig. 2**. (**A**): The gene expression ANG2/ANG1 ratio was analyzed under three tested conditions: control (untreated spheroid cells), cisPt (spheroid cells treated with 10 µM cis-platin), and [Zn(neo)(nif)$_2$] (spheroid cells treated with 10 µM [Zn(neo)(nif)$_2$]) measured in six replicates (n = 6). Changes in the ANG2/ANG1 ratio in the HME1 cell line were insignificant across all tested conditions (cisPt P = 0.9812; [Zn(neo)(nif)$_2$] P = 0.7468; cisPt vs. [Zn(neo)(nif)$_2$] P = 0.8665). Changes in the ANG2/ANG1 ratio in the 12Z cells, significant changes were observed for control vs. cisPt (P < 0.0001, ***), control vs. [Zn(neo)(nif)$_2$] (P < 0.0001, ***), and cisPt vs. [Zn(neo)(nif)$_2$] (P < 0.0001, + ++). In A2780 cells, the ANG2/ANG1 ratio changes were significant for control vs. [Zn(neo)(nif)$_2$] (P < 0.0001, ***) and cisPt vs. [Zn(neo)(nif)$_2$] (P < 0.0001, + ++), insignificant for control vs. cisPt (P = 0.1243). (**B**): The VEGF-A/TGFβ1 ratio (n = 6) showed significant changes in the HME1 model under treatment with cisPt (P < 0.0001, ***), under treatment with [Zn(neo)(nif)$_2$] (P < 0.0001, ***), and between cisPt and [Zn(neo)(nif)$_2$] treatments (P < 0.0001, + ++). In the 12Z cells treated with cisPt, a significant change was observed (P = 0.0019, **), whereas treatment with [Zn(neo)(nif)$_2$] showed an insignificant change (P = 7334). The difference between 12Z cells treated with cisPt and [Zn(neo)(nif)$_2$] was significant (P = 0.0109, +). In the A2780 cell line, significant changes were observed under treatment with cisPt (P = 0.0044, **) and treated with [Zn(neo)(nif)$_2$] (P < 0.0001, ***), compared to the control. However, the difference between A2780 cells treated with cisPt and [Zn(neo)(nif)$_2$] was insignificant (P = 0.1622). (**C**): The gene expression ratio of Nrf2/COX2 (n = 6) showed insignificant changes in the HME1 cell line under treatment with cisPt (P = 0.8172), [Zn(neo)(nif)$_2$] (P = 0.4868), and between cisPt and [Zn(neo)(nif)$_2$] treatments (P = 0.8468). In 12Z cells, significant changes were observed for control vs. [Zn(neo)(nif)$_2$] (P < 0.0001, ***) and cisPt vs. [Zn(neo)(nif)$_2$] (P < 0.0001, + ++), while the change under treatment with cisPt was insignificant (P = 0.6750). In A2780 cells, significant changes were observed for control vs. cisPt (P < 0.0001, ***), control vs. [Zn(neo)(nif)$_2$] (P < 0.0001, ***), and cisPt vs. [Zn(neo)(nif)$_2$] (P < 0.0001, + ++). (**D**): The gene expression COX2/HIF-1α ratio (n = 6) showed significant changes in the HME1 cell line for control vs. cisPt (P = 0.0217, *), under treatment with [Zn(neo)(nif)$_2$] (P < 0.0001, ***) compared to control, and between cisPt vs. [Zn(neo)(nif)$_2$] (P < 0.0001, + ++). COX2/HIF-1α ratio changes of 12Z were significant under cisPt treatment (P = 0.0001, ***), with [Zn(neo)(nif)$_2$] (P = 0.0044, **), and between tested compounds cisPt and [Zn(neo)(nif)$_2$] (P < 0.0001, + ++). The COX2/HIF-1α ratio changes in A2780 cells were insignificant for control vs. cisPt (P = 0.9844), control vs. [Zn(neo)(nif)$_2$] (P = 0.9998), and cisPt vs. [Zn(neo)(nif)$_2$] (P = 0.9806). **E:** The gene expression of CAS3/BAX ratio (n = 6) showed insignificant changes in the HME1 cell line under treatment with cisPt (P = 0.4299), [Zn(neo)(nif)$_2$] (P = 0.8530), and also between cisPt vs. [Zn(neo)(nif)$_2$] treatments (P = 0.7295). In 12Z cells, insignificant changes were found for control vs. cisPt (P = 0.8766), while significant changes were observed for control vs. [Zn(neo)(nif)$_2$] (P < 0.0001), and cisPt vs. [Zn(neo)(nif)$_2$] (P < 0.0001, + ++). In A2780 cells, the CAS3/BAX ratio remained insignificant across all tested conditions: cisPt (P = 0.9997), [Zn(neo)(nif)$_2$] (P = 0.1528), and between cisPt and [Zn(neo)(nif)$_2$] (P = 0.1168).

HME1	Nrf2 (P value, signif.)	COX2 (P value, signif.)	HIF-1α (P value, signif.)	CAS3 (P value, signif.)	BAX (P value, signif.)
control vs. cisPt	0.0071 (**) ↑	0.0028 (**) ↓	0.0223 (*) ↓	0.2321 (ns) ↓	0.0881 (ns) ↑
control vs. [Zn(neo)(nif)2]	0.0025 (**) ↑	0.0096 (**) ↓	0.1097 (ns) ↓	0.0170 (*) ↓	0.0782 (ns) ↑
cisPt vs. [Zn(neo)(nif)2]	0.1114 ↑	0.0015 (**) ↓	0.4543 (ns) ↓	0.0781 (ns) ↓	0.0704 (ns) ↑
12Z					
control vs. cisPt	0.0065 (**) ↑	0.0003 (***) ↓	0.1602 (ns) ↓	0.0013 (**) ↓	0.0073 (**) ↑
control vs. [Zn(neo)(nif)$_2$]	0.0191 (*) ↑	0.0571 (ns) ↓	0.5077 (ns) ↓	0.4635 (ns) ↑	0.4077 (ns) ↑
cisPt vs. [Zn(neo)(nif)$_2$]	0.0073 (**) ↑	0.0076 (**) ↓	0.1597 (ns) ↓	0.0016 (**) ↑	0.0180 (*) ↑
A2780					
control vs. cisPt	0.0004 (***) ↓	0.5231 (ns) ↓	0.0062 (**) ↑	0.1597 (ns) ↑	0.1452 (ns) ↑
control vs. [Zn(neo)(nif)$_2$]	0.0004 (***) ↑	0.1202 (ns) ↑	0.0033 (**) ↑	0.2337 (ns) ↑	0.0464 (*) ↑
cisPt vs. [Zn(neo)(nif)$_2$]	0.9999 (ns) ↑	0.5414 (ns) ↑	0.0023 (**) ↑	0.1557 (ns) ↑	0.0162 (*) ↑

Table 2. Significance values of Nrf2, COX2, HIF-1α, and CAS3, BAX (n = 6) under three tested conditions: control (untreated spheroid cells), cisPt (spheroid cells treated with 10 µM cis-platin), [Zn(neo)(nif)$_2$] (spheroid cells treated with 10 µM [Zn(neo)(nif)$_2$]) across three experimental 3D models.

Table 2 summarizes the individual changes in the gene expression of the monitored inflammatory (COX2, HIF-1α), antioxidant (Nrf2), and apoptotic (CAS3, BAX) factors.

Based on the detected changes in Nrf2 gene expression levels, we analyzed the gene expression of its two selected target gene products, GPx1 and SOD1 (Fig. 3). The relative gene expression of GPx1 significantly increased in all studied cell lines under both tested conditions (P < 0.001). Different conclusions were drawn for the relative gene expression of SOD1, where we observed a significant increase in expression in the HME1 cell model following treatment with [Zn(neo)(nif)$_2$] (P = 0.0188). In the 12Z cell model, a significant increase in expression was determined under the influence of both tested compounds (P < 0.0001), and in the A2780 cell model, we observed a significant increase in expression following treatment with cisPt (P < 0.0001).

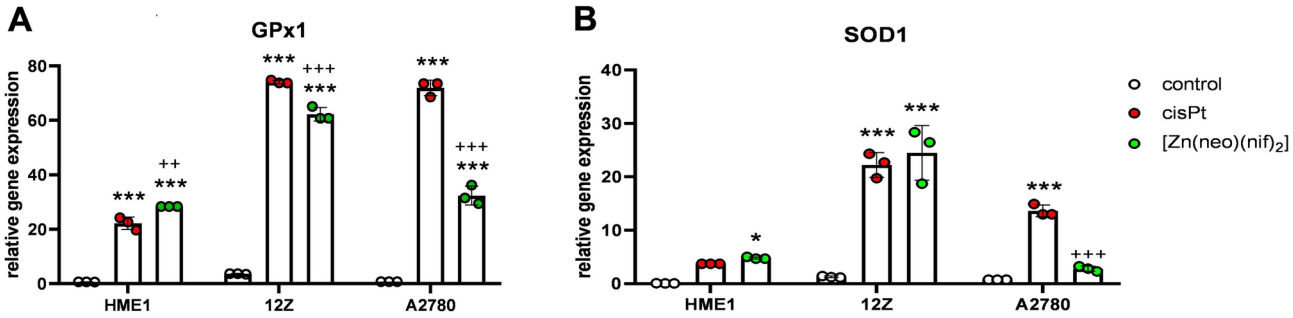

Fig. 3. (**A**): The gene expression GPx1 (n = 3) under three tested conditions: control (untreated spheroid cells), cisPt (spheroid cells treated with 10 µM cis-platin), and $[Zn(neo)(nif)_2]$ (spheroid cells treated with 10 µM $[Zn(neo)(nif)_2]$) showed a significant increase under treatment with cisPt ($P < 0.0001$, ***), $[Zn(neo)(nif)_2]$ ($P < 0.0001$, ***), and between cisPt and $[Zn(neo)(nif)_2]$ ($P = 0.0024$, ++). In 12Z cells, GPx1 expression was significantly increased under both treatment conditions, cisPt and $[Zn(neo)(nif)_2]$ ($P < 0.0001$, ***), and a significant difference was observed between cisPt vs. $[Zn(neo)(nif)_2]$ ($P < 0.0001$, +++). The A2780 model also showed a significant increase under both treatment conditions ($P < 0.0001$, ***), as well as a significant difference between cisPt and $[Zn(neo)(nif)_2]$ ($P < 0.0001$, +++). (**B**): The gene expression SOD1 (n = 3) under the same three tested conditions: control (untreated spheroid cells), cisPt (spheroid cells treated with 10 µM cis-platin), and $[Zn(neo)(nif)_2]$ (spheroid cells treated with 10 µM $[Zn(neo)(nif)_2]$) indicated an insignificant increase in HME1 cells under treatment with cisPt ($P = 0.0736$), a significant increase under treatment with $[Zn(neo)(nif)_2]$ ($P = 0.0188$), and no significant change between cisPt and $[Zn(neo)(nif)_2]$ ($P = 0.7808$). In 12Z cells, a significant increase in SOD1 expression was observed under both cisPt and $[Zn(neo)(nif)_2]$ ($P < 0.0001$, ***), while the difference between cisPt and $[Zn(neo)(nif)_2]$ was insignificant ($P = 0.3403$). In the A2780 model, SOD1 gene expression was significantly increased under treatment with cisPt ($P < 0.0001$, ***), increased insignificantly under treatment with $[Zn(neo)(nif)_2]$ ($P = 0.4126$), and showed a significant difference between cisPt and $[Zn(neo)(nif)_2]$ treatments ($P < 0.0001$, +++).

HME1	GPx1 (P value, signif.)	SOD1 (P value, signif.)
control vs. cisPt	< 0.0001 (***) ↑	0.0736(ns) ↑
control vs. $[Zn(neo)(nif)_2]$	< 0.0001 (***) ↑	0.0188 (*) ↑
cisPt vs. $[Zn(neo)(nif)_2]$	0.0024 (**) ↑	0.7808 (ns) ↑
12Z		
control vs. cisPt	< 0.0001 (***) ↑	< 0.0001 (***) ↑
control vs. $[Zn(neo)(nif)_2]$	< 0.0001 (***) ↑	< 0.0001 (***) ↑
cisPt vs. $[Zn(neo)(nif)_2]$	< 0.0001 (***) ↓	0.3403 (ns) ↑
A2780		
control vs. cisPt	< 0.0001 (***) ↑	< 0.0001 (***) ↑
control vs. $[Zn(neo)(nif)_2]$	< 0.0001 (***) ↑	0.4126 (ns) ↑
cisPt vs. $[Zn(neo)(nif)_2]$	< 0.0001 (***) ↓	< 0.0001 (***) ↓

Table 3. Significance values of GPx1 and SOD1 (n = 3) under three tested conditions: control (untreated spheroid cells), cisPt (spheroid cells treated with 10 µM cis-platin), $[Zn(neo)(nif)_2]$ (spheroid cells treated with 10 µM $[Zn(neo)(nif)_2]$) across three experimental 3D model cells.

Table 3 summarizes the individual changes in the gene expression of the monitored antioxidant factors (GPx1 and SOD1).

Expression of angiogenic and inflammatory microRNAs

To further support our findings on the potential effects of our compounds on inflammatory and angiogenic pathways, we analyzed the delicate balance between pro-angiogenic (miR-23a, -133b, let-7c) and anti-angiogenic (miR-206, -376a) microRNA levels, which play a crucial role in the physiological regulation of vascular network formation and immune response.

MicroRNAs are small yet highly significant molecules that regulate gene expression and control cellular metabolism. Our focus was on determining the ratio of target miRNAs to selected angiogenic (VEGF-A, TGF-β1), antioxidant (Nrf2), and inflammatory factors (COX2, HIF-1α). The miRNA/mRNA ratio provides insight into the extent of miRNA influence on the expression of the corresponding mRNA, as miRNAs can promote degradation and inhibit its translation into protein. This ratio can, therefore, help predict the direction of cellular metabolism.

We determined the ratio of miR-206, -23a, -376a, -133b, and let-7c against VEGF-A, as it has previously described that these miRs influence the expression of VEGF-A and angiogenesis. We observed a significant increase in the ratio of miR-206/VEGF-A (Fig. 4A) in the HME1 model treated with cisPt ($P < 0.0001$). A significant decrease in miR-206/VEGF-A ratio was observed in 12Z cells treated with both cisPt ($P < 0.00001$) and [Zn(neo)$(nif)_2$] ($P < 0.0001$). In A2780 cells, we observed a significant decrease in mi-206/VEGF-A ratio only in the group treated with [Zn(neo)$(nif)_2$] ($P = 0.0021$).

An insignificant increase in the miR-23a/VEGF-A ratio (Fig. 4B) was observed in HME1 cells treated with cisPt ($P < 0.0001$). In the 12Z model, a significant decrease was observed under both treatment conditions, cisPt ($P < 0.0001$) and [Zn(neo)$(nif)_2$] ($P < 0.0001$), while the A2780 cell model showed no significant changes.

The miR-133b/VEGF-A ratio (Fig. 4D) showed a significant increase in HME1 cells treated again with cisPt ($P < 0.0001$). In 12Z cells, a significant decrease in miR-376a/VEGF-A ratio was observed under both treatment conditions, cisPt ($P < 0.0001$) and [Zn(neo)$(nif)_2$] ($P < 0.0001$). The A2780 cells did not show significant changes in the miR-376a/VEGF-A ratio.

A significant increase in the miR-133b/VEGF-A ratio was observed in HME1 cells ($P < 0.0001$), while in 12Z cells, a significant decrease was determined under both treatments ($P < 0.0001$). In the A2780 model, a significant decrease was observed with cisPt treatment ($P = 0.0358$) and [Zn(neo)$(nif)_2$] ($P = 0.0015$).

We identified a significant increase in the let-7c/VEGF-A ratio in the HME1 model treated with cisPt ($P < 0.0001$). The 12Z cell model showed a significant decrease in the let-7c/VEGF-A ratio under both treatment conditions ($P < 0.0001$), as did the A2780 cells, which exhibited the same significant decrease ($P < 0.0001$) under both tested conditions (Fig. 4E).

The expression of miR-133b and let-7c significantly impacts the expression of TGF-β1, as previously described[6,34]. The levels of TGF-β1 and miR-133b, along with let-7c, influence the epithelial-mesenchymal transition, which is characteristic of promoted endometriosis. The calculated ratio of miR-133b/TGF-β1 showed a significant increase in the HME1 model under both treatment conditions: cisPt (0.0009) and [Zn(neo)$(nif)_2$] ($P < 0.0001$). The 12Z model showed a significant decrease under [Zn(neo)$(nif)_2$] treatment ($P = 0.0045$), and the A2780 model exhibited a significant decrease with cisPt treatment ($P = 0.0301$) and [Zn(neo)$(nif)_2$] treatment (0.0100) as well (Fig. 5A).

We observed a significant increase in the let-7c/TGF-β1 ratio in HME1 cells treated with cisPt ($P = 0.004$) and [Zn(neo)$(nif)_2$] ($P = 0.0002$). In the 12Z model, the let-7c/TGF-β1 ratio significantly decreased under both treatment conditions (cisPt $P = 0.0201$; [Zn(neo)$(nif)_2$] $P = 0.0043$). The A2780 model also showed a significant decrease in the let-7c/TGF-β1 ratio under both treatment conditions (cisPt $P = 0.0066$; [Zn(neo)$(nif)_2$] $P = 0.0041$) (Fig. 5B).

MiR-206 recognizes the binding site of HIF-1α and can regulate the HIF transcription factor. It can inhibit cell proliferation and extracellular matrix accumulation by targeting HIF-1α. Based on the direct effect of miR-206 on HIF-1α, we performed an additional calculation of the miR-206/HIF-1α ratio, which showed a significant increase in HME1 cells treated with cisPt ($P < 0.0001$) and [Zn(neo)$(nif)_2$] ($P = 0.0039$). In contrast, 12Z cells exhibited a significant decrease under treatment with [Zn(neo)(nif)2] ($P = 0.0002$), while A2780 cells treated with cisPt showed a significant increase ($P = 0.0023$) (Fig. 5C).

Nrf2-dependent miR-206 plays an essential role in cell metabolism by targeting the pentose phosphate pathway, leading to the inhibition of proliferation. We observed a significant decrease in the miR-206/Nrf2 ratio in the 12Z model under cisPt treatment ($P = 0.0013$) and [Zn(neo)$(nif)_2$] treatment ($P = 0.0003$). Similarly, A2780 cells exhibited a significant decrease under treatment with both compounds (cisPt $P = 0.0047$; [Zn(neo)$(nif)_2$] $P = 0.0021$) (Fig. 5D). In contrast, HME1 cells showed a slight, non-significant reduction in miR-206/Nrf2 under treatment of both tested conditions. This reduction may reflect elevated antioxidant activity, leading to increased Nrf2 levels, which could, in turn, decrease miR-206 expression under studied conditions.

In the HME1 spheroids, we observed a significant elevation of the angiogenesis-promoting miR-133b (cisPt $P = 0.0005$; [Zn(neo)$(nif)_2$] $P = 0.0030$) (Figure S2A), along with a considerable upregulation of the angiogenesis-inhibiting miR-206 (cisPt $P = 0.0070$; [Zn(neo)$(nif)_2$] $P = 0.0187$) (Figure S2B). The levels of the other miRs did not show considerable changes in either treatment group.

In the 3D model of the 12Z cell line (Figure S2C), a significant decrease was observed in the level of the angiogenesis-promoting miR-23a (cisPt $P = 0.0471$; [Zn(neo)$(nif)_2$] $P = 0.0149$) and let-7c (cisPt $P < 0.0001$; [Zn(neo)$(nif)_2$] $P = 0.0001$) (Figure S2D). The expression levels of the remaining target miRs did not show significant changes in either treatment group.

Spheroids of A2780 (Figure S2E) exhibited a significant downregulation of the angiogenesis-promoting miR-133b ([Zn(neo)$(nif)_2$] $P = 0.0470$), a decrease in the proangiogenic let-7c (cisPt $P = 0.0019$; [Zn(neo)$(nif)_2$] $P = 0.0002$), and a significant upregulation of the angiogenesis-inhibiting miR-376 ([Zn(neo)$(nif)_2$] $P = 0.0006$) (Figure S2F). The levels of other miRs did not show considerable changes in either treatment group.

Angiogenic, inflammatory, and antioxidant protein expression

Gene expression typically predicts the corresponding protein levels; however, these levels may be influenced by post-transcriptional and post-translational modifications, potentially leading to unexpected protein levels. We analyzed the protein levels of angiogenic proteins VEGF-A and TGF-β1, the inflammatory marker COX2, and the antioxidant marker Nrf2 (both in its total and phosphorylated (active) form) (Table 4).

To evaluate protein levels under tested conditions, we calculated the VEGF-A/TGF-β1 ratio, the Nrf2 active/COX2 ratio, and the Nrf2 active/Nrf2 ratio. In the control model of HME1 cells, the VEGF-A/TGF-β1 ratio showed a non-significant decrease (Fig. 6A). In the 12Z cell model, a significant increase was observed following treatment with cisPt ($P < 0.0001$), while treatment with [Zn(neo)$(nif)_2$] resulted in a non-significant decrease ($P = 0.1781$). In A2780 cells, a significant increase was observed with cisPt ($P = 0.0487$), whereas a significant decrease was noted with [Zn(neo)$(nif)_2$] treatment ($P = 0.0451$).

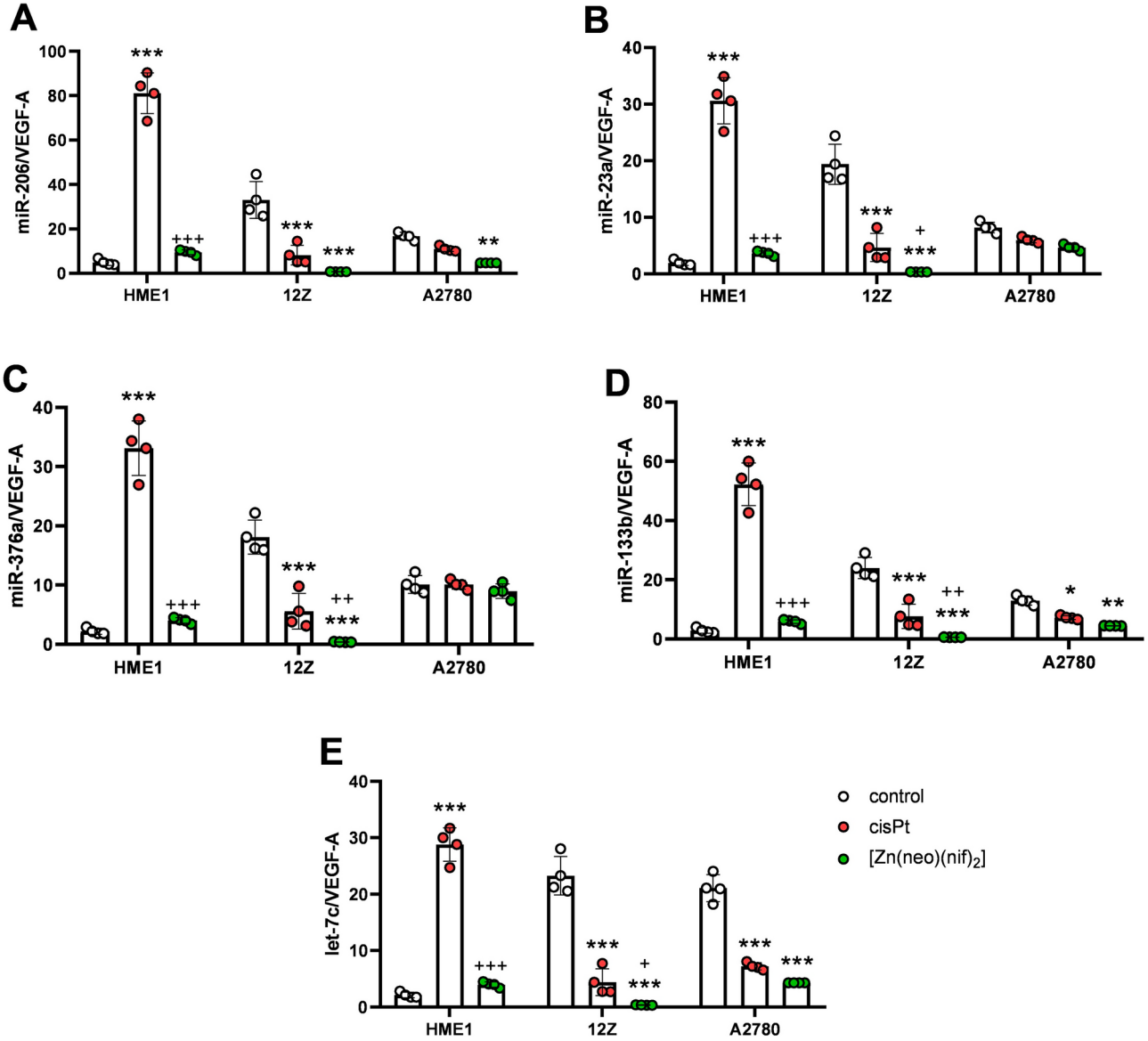

The Nrf2 active/COX2 ratio showed a significant increase only in the A2780 model treated with cisPt ($P = 0.0045$) (Fig. 6B), while no considerable changes were observed in the other tested models (HME1 and 12Z).

The regulatory action of the Nrf2 protein is exerted only in its phosphorylated form[35]. Therefore, we analyzed the ratio of phosphorylated (active) Nrf2 to its total level in the tested groups (Fig. 6C). The results revealed a significant decrease in the Nrf2 active/Nrf2 ratio in A2780 cells treated with cisPt ($P = 0.0366$). No considerable change was observed under any tested conditions, including treatment with cisPt or [Zn(neo)$(nif)_2$].

The key regulatory factors COX2 and TGF-β1 cooperate in the development of inflammation. The COX2/TGF-β1 ratio showed a significant increase in 12Z cells treated with cisPt ($P < 0.0001$) (Fig. 6D) and in A2780 cells treated with [Zn(neo)$(nif)_2$] ($P = 0.0432$).

VEGF-A and Nrf2 are pivotal in regulating angiogenesis and cellular response to oxidative stress. Their reciprocal relationship is illustrated in Fig. 6E. In the HME1 model, the VEGF-A/Nrf2 ratio significantly decreased under treatment with [Zn(neo)$(nif)_2$] ($P = 0.0254$). In the 12Z model, this ratio significantly decreased under treatment with both cisPt ($P = 0.0017$) and [Zn(neo)$(nif)_2$] ($P = 0.0123$). In the A2780 model, a significant decrease was observed under treatment with [Zn(neo)$(nif)_2$] ($P = 0.0225$).

The final protein ratio analyzed was the TGF-β1/Nrf2 ratio (Fig. 6F), which reflects the regulation of oxidative stress and inflammation at the cellular level. In the 12Z model, a significant decrease was observed under treatment with [Zn(neo)$(nif)_2$] ($P < 0.0001$). Similarly, in the A2780 model, a significant decrease was observed under treatment with cisPt ($P = 0.0097$).

Mitochondrial Ca^{2+}, H_2O_2 levels, and cytosolic levels of Ca^{2+}

Mitochondrial calcium overload, caused by Ca^{2+} influx released from the endoplasmic reticulum under stress conditions, stimulates immune responses and ultimately leads to apoptosis. For live-imaging measurements, we selected the epithelial cell lines HME1 and 12Z based on the gene expression results of angiogenic and apoptotic factors. Excessive mitochondrial calcium accumulation can trigger the opening of the mitochondrial

◀**Fig. 4**. (**A**): The gene expression miR-206/VEGF-A ratio (n = 4) was analyzed under three tested conditions: control (untreated spheroid cells), cisPt (spheroid cells treated with 10 µM cis-platin), and $[Zn(neo)(nif)_2]$ (spheroid cells treated with 10 µM $[Zn(neo)(nif)_2]$). In HME1 cells, significant changes were found under treatment with cisPt ($P < 0.0001$, ***), while changes under $[Zn(neo)(nif)_2]$ treatment were insignificant ($P = 0.3425$). A significant difference was observed between cisPt and $[Zn(neo)(nif)_2]$ ($P < 0.0001, + + +$). In 12Z cells, significant changes were found for control vs. cisPt ($P < 0.0001$, ***) and control vs. $[Zn(neo)(nif)_2]$ ($P < 0.0001$, ***), while the difference between cisPt. Vs. $[Zn(neo)(nif)_2]$ was insignificant ($P = 0.0644$). In A2780 cells, the changes were insignificant under cisPt treatment ($P = 0.1882$|, significant under $[Zn(neo)(nif)_2]$ treatment ($P = 0.0021$, **), and insignificant change cisPt vs. $[Zn(neo)(nif)_2]$ ($P = 0.1341$) (**B**): The gene expression miR-23a/VEGF-A ratio showed significant changes in HME1 under treatment with cisPt ($P < 0.0001$, ***), insignificant changes under $[Zn(neo)(nif)_2]$ treatment ($P = 0.4761$), and significant differences between cisPt and $[Zn(neo)(nif)_2]$ treatments ($P < 0.0001, + + +$). In 12Z cells, significant changes were observed under both cisPt and $[Zn(neo)(nif)_2]$ treatments ($P < 0.0001$, ***), as well as between cisPt and $[Zn(neo)(nif)_2]$ ($P = 0.0152, +$). In A24780 cells, the ratio showed insignificant changes across all tested conditions: cisPt ($P = 0.2920$), $[Zn(neo)(nif)_2]$ ($P = 0.0524$), and between cisPt and $[Zn(neo)(nif)_2]$ ($P = 0.6294$). (**C**): The gene expression miR-376a/VEGF-A ratio showed significant changes in HME1 under treatment with cisPt ($P < 0.0001$, ***), insignificant changes under treatment with $[Zn(neo)(nif)_2]$ ($P = 0.4752$), and significantdifferences between cisPt and $[Zn(neo)(nif)_2]$ treatments ($P < 0.0001, + + +$). In 12Z cells, significant changes were observed under both cisPt and $[Zn(neo)(nif)_2]$ treatments ($P < 0.0001$, ***), as well as between and $[Zn(neo)(nif)_2]$ ($P = 0.0066, + +$). In the A2780 cells, no significant changes were observed across all tested conditions: cisPt ($P = 0.9996$), $[Zn(neo)(nif)_2]$ ($P = 0.7412$), and cisPt vs. $[Zn(neo)(nif)_2]$ ($P = 0.7567$). (**D**): The gene expression miR-133b/VEGF-A ratio showed significant changes in HME1 cells under treatment with cisPt ($P < 0.0001$, ***), insignificant changes under $[Zn(neo)(nif)_2]$ treatment ($P = 0.3538$), and significant difference for cisPt vs. $[Zn(neo)(nif)_2]$ ($P < 0.0001, + + +$). In 12Z cells, the ratio significantly changed under both cisPt and $[Zn(neo)(nif)_2]$ treatment ($P < 0.0001$, ***), as well as between cisPt and $[Zn(neo)(nif)_2]$ ($P = 0.0088, + +$). In A2780 cells, significant changes were observed under cisPt treatment ($P = 0.0358$, *), $[Zn(neo)(nif)_2]$ ($P = 0.0015$, **), and insignificant changes between cisPt and $[Zn(neo)(nif)_2]$ ($P = 0.4129$). **E:** The gene expression let-7c/VEGF-A ratio showed significant changes in HME1 for control vs. cisPt ($P < 0.0001$, ***), insignificant changes for control vs. $[Zn(neo)(nif)_2]$ ($P = 0.3580$), and significant differences between cisPt and $[Zn(neo)(nif)_2]$ treatments ($P < 0.0001, + + +$). In 12Z cells, significant changes were observed under both cisPt and $[Zn(neo)(nif)_2]$ treatments ($P < 0.0001$, ***), as well as between cisPt and $[Zn(neo)(nif)_2]$ ($P = 0.0147, +$). In A2780 cells, significant changes were found for control vs. cis-Pt ($P < 0.0001$, ***) and control vs. $[Zn(neo)(nif)_2]$ ($P < 0.0001$, ***), while changes between cisPt vs. $[Zn(neo)(nif)_2]$ were insignificant ($P = 0.0913$).

permeability transition pore, resulting in the release of calcium from the mitochondria into the cytosol, serving as an indicator of apoptotic processes in the cell.

We quantified basal mitochondrial Ca^{2+} levels using the genetically encoded mitochondrial Ca^{2+} biosensor 4mtD3cpv. A significant increase in mitochondrial Ca^{2+} levels was observed in control HME1 cells in response to treatment with cisPt ($P = 0.0069$) and $[Zn(neo)(nif)_2]$ ($P = 0.0001$) (Fig. 7A). Additionally, a significant increase in the mitochondrial Ca^{2+} level was detected in endometriotic 12Z cells treated with $[Zn(neo)(nif)_2]$ ($P < 0.0001$), whereas no effect was observed with cisPt treatment (Fig. 7D).

To further investigate, cytosolic free Ca^{2+} levels were measured using the Ca^{2+} dye Fura-2. Significant changes were observed in both tested epithelial cell lines (HME1, 12Z). In HME1 cells, basal cytosolic Ca^{2+} levels significantly changed in response to $[Zn(neo)(nif)_2]$ ($P < 0.0001$) (Fig. 7B). Similarly, in 12Z cells, cytosolic Ca^{2+} levels significantly increased in response to cisPt ($P < 0.0001$) as well as $[Zn(neo)(nif)_2]$ ($P < 0.0001$) (Fig. 7E).

Mitochondrial metabolism is closely associated with Ca^{2+} and ROS levels. To assess mitochondrial ROS levels, we utilized the genetically encoded mitoHyPer7 biosensor. A significant increase in ROS was observed in 12Z endometriotic cells following treatment with $[Zn(neo)(nif)_2]$ ($P = 0.0126$), whereas the increase in HME1 cells was not statistically significant (Fig. 7C, F).

Discussion

Angiogenesis is a physiological process that facilitates the formation of the primary vascular network necessary for tissue growth and repair[36]. It regulates oocyte maturation, the development of functional corpora lutea, and uterine endometrial growth and decidualization[37]. Disruption of this process due to the constant activation of angiogenic factors can lead to excessive vessel growth, contributing to the development and progression of endometriosis and its potential malignant transition[38].

The complex interplay between the immune system, hormones, microelements, and genetic factors significantly influences the development and progression of endometriosis[39]. Transcription factors such as ZNFs and miRs play a dual role; they can reduce inflammation via immunosuppression, thereby promoting the spread and invasiveness of the condition[40]. Additionally, they can inhibit apoptotic cell death[41] in endometriotic cells and wild-type tumors, such as endometrioid adenocarcinoma, ovarian cancer, or cervical squamous cell carcinoma[42].

The regulatory gene sequences of angiogenic factors can vary depending on the specificity of the target ZNFs. For example, ZNF471 has been shown to regulate the expression of EMT-related markers and transcription factors involved in angiogenesis, cellular migration, and vasculogenic mimicry[43]. Conversely, ZNF24 has been reported to repress VEGF transcription[44]. ZNF3 is known to be highly expressed in colorectal carcinoma cells[45],

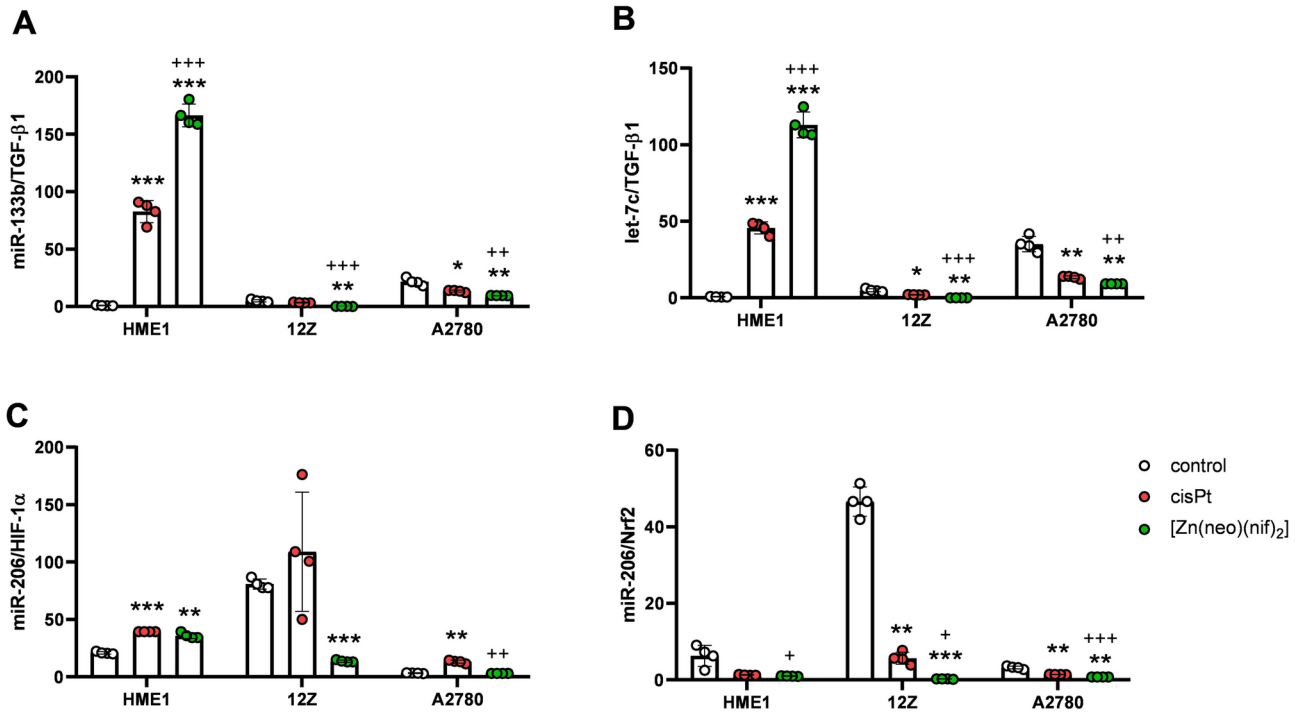

Fig. 5. (**A**): The gene expression miR-133b/TGF-β1 ratio (n = 4) was analyzed under three tested conditions: control (untreated spheroid cells), cisPt (spheroid cells treated with 10 μM cis-platin), and $[Zn(neo)(nif)_2]$ (spheroid cells treated with 10 μM $[Zn(neo)(nif)_2]$). Significant changes in the miR-133b/TGF-β1 ratio were observed in HME1 cells under treatment with cisPt (P = 0.0009, ***), with $[Zn(neo)(nif)_2]$ (P < 0.0001, ***), and between cisPt and $[Zn(neo)(nif)_2]$ (P = 0.0008, ***). In 12Z cells, the ratio showed an insignificant change under treatment with cisPt (P = 0.1162), a significant change under treatment with $[Zn(neo)(nif)_2]$ (P = 0.0045), a significant change between cisPt and $[Zn(neo)(nif)_2]$ (P = 0.0005, + + +). In A24780 cells, a significant change was observed under treatment with cisPt (P = 0.0301, *), with $[Zn(neo)(nif)_2]$ (P = 0.0100, **), and between cisPt and $[Zn(neo)(nif)_2]$ (P = 0.0040, + +). (**B**): The gene expression let-7c/TGF-β1 ratio (n = 4) in HME1 cells showed significant changes for control vs. cisPt (P = 0.0004, ***), control vs. $[Zn(neo)(nif)_2]$ (P = 0.0002, ***), and cisPt vs. $[Zn(neo)(nif)_2]$ (P = 0.0008, + + +). In 12Z cells, significant changes were observed under treatment with cisPt (P = 0.0201), with $[Zn(neo)(nif)_2]$ (P = 0.0043, **), and between cisPt and $[Zn(neo)(nif)_2]$ (P = 0.0001, + + +). In A2780 cells, significant changes were found under treatment with cisPt (P = 0.0066, **), with $[Zn(neo)(nif)_2]$ (P = 0.0041), and between the two treatments (P = 0.0044, + +). (**C**): The gene expression miR-206/HIF-1α ratio (n = 4) showed a significant elevation in HME1 cells under treatment with cisPt (P < 0.0001, ***), with $[Zn(neo)(nif)_2]$ (P = 0.0039, **), and insignificant change between cisPt and $[Zn(neo)(nif)_2]$ (P = 0.1324). In 12Z cells, the ratio was insignificantly increased under treatment with cisPt (P = 0.5895) and significantly decreased under treatment with $[Zn(neo)(nif)_2]$ (P = 0.0002, ***). The difference between cisPt and $[Zn(neo)(nif)_2]$ treatment was insignificant (P = 0.0665). In A2780 cells, a significant increase was observed for control vs. cisPt (P = 0.0023, **), an insignificant change for control and $[Zn(neo)(nif)_2]$ (P = 0.4254), and a significant difference between cisPt and $[Zn(neo)(nif)_2]$ treatments (P = 0.0012, + +). (**D**): The gene expression miR-206/Nrf2 ratio (n = 4) in HME1 model showed an insignificant decrease under treatment with cisPt (P = 0.0692), an insignificant change under treatment with $[Zn(neo)(nif)_2]$ (P = 0.0659), and a significant decrease between cisPt vs. $[Zn(neo)(nif)_2]$ (P = 0.0233, +). In 12Z cells, the ratio significantly decreased under treatment with cisPt (P = 0.0013, **), with $[Zn(neo)(nif)_2]$ (P = 0.0003, ***), and between cisPt and $[Zn(neo)(nif)_2]$ (P = 0.0123, +). In A2780 cells, a significant decrease was observed under treatment with cisPt (P = 0.0047, **), with $[Zn(neo)(nif)_2]$ (P = 0.0021, **), and a highly significant change between cisPt and $[Zn(neo)(nif)_2]$ (P < 0.0001, + + +).

where it plays a role in cellular proliferation, migration, and invasion. If the $[Zn(neo)(nif)_2]$ intercalates into the ZNF3 sequence, it could exert a suppressive effect on target genes, which aligns with the gene expression changes observed in 12Z and A2780 cell lines.

The obtained data indicate that the $[Zn(neo)(nif)_2]$ complex may influence gene regulation, as evidenced by its impact on expression of target gene associated with the promotion or suppression of angiogenesis (e.g., mRNA of ANG1, ANG2, TGF-β1, HIF-1α, COX2, Nrf2, BAX, and CAS3), on the expression of micro-RNA (e.g., miR-133b, miR-206, miR-376, miR-376, or let-7c), as well as on protein expression related to angiogenesis (e.g., COX2, VEGF-A, TGF-β1, and Nrf2). The molecular conformation of the complex suggests the possibility of intercalation, where the aromatic neocuproine ligand may intercalate between DNA base pairs, potentially stabilized by π-π stacking interactions, hydrogen bonding, van der Waals forces, and hydrophobic interactions[46].

HME1	VEGF-A (P value, signif.)	TGF-β1 (P value, signif.)	COX2 (P value, signif.)	Nrf2 (P value, signif.)	Nrf2 active (P value, signif.)
control vs. cisPt	0.0528 (ns) ↓	0.0159 (*) ↓	0.3151 (ns) ↑	0.1338 (ns) ↑	0.7100 (ns) ↓
control vs. $[Zn(neo)(nif)_2]$	0.0462 (*) ↓	0.6167 (ns) ↑	0.3151 (ns) ↑	0.1131 (ns) ↑	0.9862 (ns) ↑
cisPt vs. $[Zn(neo)(nif)_2]$	0.0445 (*) ↓	0.0246 (*) ↑	0.3151 (ns) ↓	0.3792 (ns) ↓	0.2154 (ns) ↑
12Z					
control vs. cisPt	0.0496 (*) ↓	< 0.0001 (***) ↓	0.0524 (ns) ↑	0.1121 (ns) ↓	0.8652 (ns) ↓
control vs. $[Zn(neo)(nif)_2]$	0.2219 (ns) ↓	0.3118 (ns) ↑	0.0049(**) ↑	0.7900 (ns) ↑	0.0547 (ns) ↑
cisPt vs. $[Zn(neo)(nif)_2]$	0.0228 (*) ↑	0.0033 (**) ↑	0.3151 (ns) ↑	0.3380 (ns) ↑	0.0789 (ns) ↑
A2780					
control vs. cisPt	0.0573 (ns) ↑	(ns)	0.3859 (ns) ↓	0.8915 (ns) ↑	0.0299 (*) ↑
control vs. $[Zn(neo)(nif)_2]$	0.0342 (*) ↓	(ns)	0.1060 (ns) ↑	0.1880 (ns) ↑	0.8807 (ns) ↑
cisPt vs. $[Zn(neo)(nif)_2]$	0.0158 (*) ↓	(ns)	0.0203 (*) ↑	0.2466 (ns) ↑	0.0008 (***) ↑

Table 4. Significance values of protein levels (VEGF-A, TGF-β1, Nrf2, phosphorylated Nrf2 = Nrf2 active) (n = 3) under three tested conditions: control (untreated spheroid cells), cisPt (spheroid cells treated with 10 µM cis-platin), $[Zn(neo)(nif)_2]$ (spheroid cells treated with 10 µM $[Zn(neo)(nif)_2]$) across three experimental 3D model cells.

Although providing a definite explanation is challenging, the observed binding specificity towards the ZnF3-7 sequence might involve the preference of specific base pair sequences (e.g., C-G), as suggested by recent computational studies on aromatic organic molecules[47]. Since intercalation of the $[Zn(neo)(nif)_2]$ complex induces structural changes[48] in the ZnF3-7 sequence, it may prevent ZnF3 from binding to the major groove[49], thereby altering gene expression. Recognizing the ZnF3-7 sequence, where zinc-finger proteins bind, plays a crucial role in regulating gene expression[50], which might be a key aspect of the studied complex's mechanism of action at the cellular level.

Significant changes in TGF-β1 expression were observed in the monolayer model of cell lines used in the experiment (Table S3), with increased levels in endometriotic 12Z cells treated with cisPt and $[Zn(neo)(nif)_2]$, and decreased levels in endometriotic adenoma A2748 cells treated with same compounds. It is well known that TGF-β1 acts as a potent immunosuppressor by regulating the proliferation and survival of immune system cells and inducing cell type-specific apoptosis[51]. Additionally, TGF-β1 is a target of microRNA let-7c, which also regulates HIF-1α, estrogen receptor α, and several other genes involved in angiogenesis, cell cycle regulation, and signaling pathways[34].

Let-7c can also exhibit oncogenic effects, as it is highly expressed in ovarian cancers with poor prognosis and decreased overall survival[52]. Both VEGF-A and TGF-β1 play crucial roles in angiogenesis but have opposing effects on endothelial cells. We observed a decreasing trend in the let-7c/TGF-β1 ratio in the 12Z and A2780 cell models (Fig. 4B), which could be attributed to the apoptosis-inducing properties of TGF-β1[53]. Conversely, an increased let-7c/TGF-β1 ratio was observed in HME1 cells. It is well known that let-7c has the ability to inhibit the TGF-β1 expression. A decreased level of let-7c may lead to TGF-β1-mediated induction of fibrosis effectors (e.g., collagen I), potentially predicting disease progression. On the other hand, studies demonstrated that microRNAs of the let7-family can affect angiogenesis by modulating TGF-β1 signaling. This could reflect a similar effect to that of let-7f., which has been linked to the activation of the anti-angiogenic TGF-β1/ALK5 pathway[54]. Additionally, the observed elevation in the miR-133b/TGF-β1 ratio (Fig. 4A) in HME1 cells is significant, as miR-133b functions as an oncogene suppressor by regulating TGF-β1 receptor I and II[55]. Interestingly, the miR-133b/TGF-β1 ratio decreased, which could be explained by the fact that TGF-β1 can act as both an oncogenic and a tumor-suppressive agent, depending on the tumor stage and type[56].

TGF-β1 can upregulate COX2 expression, leading to increased production of prostaglandin E2. This, in turn, influences the COX2 pathway and may induce invasiveness in cooperation with oncogenic signals[57]. This phenomenon could explain the increased COX2/TGF-β11 protein ratio (Fig. 6D). Further research has demonstrated that TGF-β1 can elicit an Nrf2-mediated antioxidant response, contributing to its anti-inflammatory properties. For instance, the TGF-β1's ability to induce Nrf2 activity has been associated with protection against vascular wall rupture[58]. On the other hand, Nrf2 has been shown to counteract TGF-β1-mediated growth inhibition, suggesting that Nrf2 may influence the pro-tumorigenic functions of TGF-β1[59]. We analyzed the decreased TGF-β1/Nrf2 ratio in 12Z and A2780 cells under treatment with cisPt (Fig. 6F), which could represent its tumorigenic action in cooperation with COX2 and VEG-A levels.

Another significant target, VEGF-A, which protects endothelial cells from apoptosis[53], was unexpectedly elevated in the control HME1 cell line and showed an insignificant downregulation in the 12Z and A2780 cell lines (Table S3). Given that the simultaneous overexpression of VEGF-A and TGF-β1 are associated with poorer cancer prognoses[43], we analyzed the gene expression ratio of those two markers. The VEGF-A/TGF-β1 ratio (Figs. 2B, 6A) decreased only in the 12Z cell line after treatment with $[Zn(neo)(nif)_2]$, suggesting a potentially better prognosis. However, it has been reported that TGF-β1 suppresses VEGF-A-mediated angiogenesis in colon cancer metastasis[61], despite the fact that aberrant TGF-β1 expression is critical in the development of endometriosis, which shares several parallels with tumorigenesis[62]. We observed an increase in the VEGF-A/TGF-β1 ratio in both the A2780 and HME1 models, which may indicate the suppression of VEGF-A-mediated angiogenesis. The reciprocal interaction between VEGF-A and Nrf2 can drive a positive feedback loop that

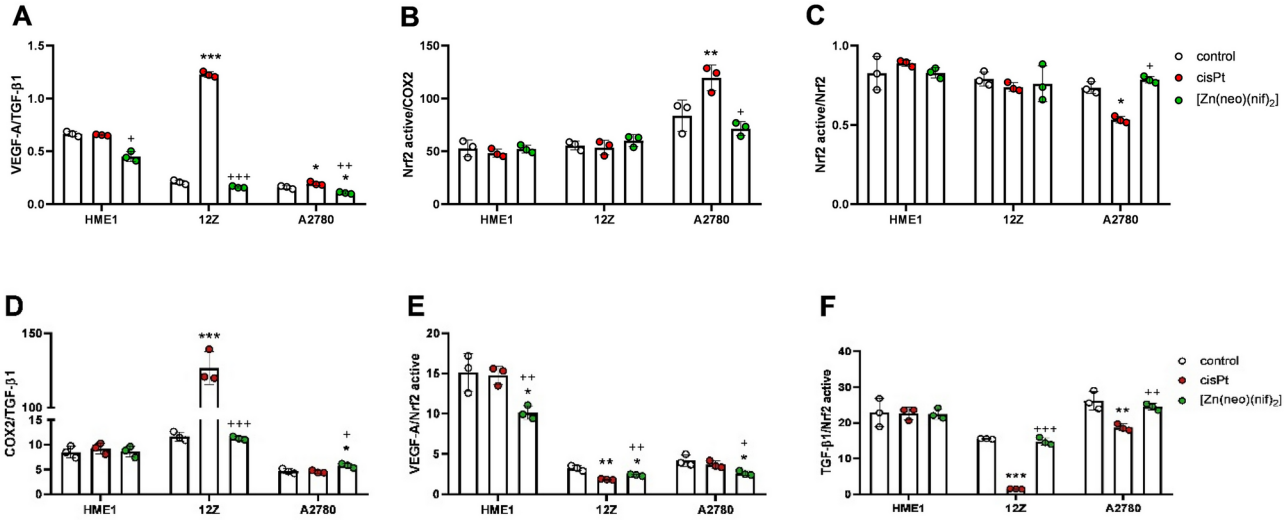

Fig. 6. The protein levels in the cultivation media were analyzed in triplicates (n = 3) across three tested conditions: control (untreated spheroid cells), cisPt (spheroids treated with 10 μM cis-platin), $[Zn(neo)(nif)_2]$ (spheroids treated with 10 μM $[Zn(neo)(nif)_2]$). (**A**): The VEGF-A/TGF-β1 protein expression ratio in HME1 showed an insignificant decrease under treatment with cisPt (P = 0.6274) and $[Zn(neo)(nif)_2]$ (P = 0.0617), but a significant change was observed between cisPt and $[Zn(neo)(nif)_2]$ treatments (P = 0.0391, +). In 12Z cells, a significant increase was detected for control vs. cisPt (P < 0.0001, ***), an insignificant decrease for control vs. $[Zn(neo)(nif)_2]$ (P = 0.1781), and a significant difference between cisPt and $[Zn(neo)(nif)_2]$ (P < 0.0001, + + +). In the A2780 model, a significant increase was observed under treatment with cisPt (P = 0.0487, *), $[Zn(neo)(nif)_2]$ (P = 0.0451, *), and between cisPt and $[Zn(neo)(nif)_2]$ treatments (P = 0.0097, + +). (**B**): The Nrf2 active/COX2 protein expression ratio in HME1 showed an insignificant decrease under treatment with cisPt (P = 0.4140) and $[Zn(neo)(nif)_2]$ (P = 0.9889), with no significant change between cisPt and $[Zn(neo)(nif)_2]$ (P = 0.1881). In 12Z cells, an insignificant decrease was observed for control vs. cisPt (P = 0.5736), an insignificant increase for control vs. $[Zn(neo)(nif)_2]$ (P = 0.1005), and an insignificant difference between cisPt and $[Zn(neo)(nif)_2]$ (P = 0.0664). In the A2780 model, a significant increase was observed under treatment with cisPt (P = 0.0045, **), an insignificant decrease with $[Zn(neo)(nif)_2]$ (P = 0.2413), and a significant difference between cisPt and $[Zn(neo)(nif)_2]$ (P = 0.0127, +). (**C**): The Nrf2 active/Nrf2 protein expression ratio in HME1 showed an insignificant increase under treatment with cisPt (P = 0.5666) and $[Zn(neo)(nif)_2]$ (P = 0.9994), as well as between cisPt and $[Zn(neo)(nif)_2]$ treatments (P = 0.1857). In 12Z cells, an insignificant decrease was observed for control vs. cisPt (P = 0.4890) and for control vs. $[Zn(neo)(nif)_2]$ (P = 0.9323), as well as between both tested conditions cisPt and $[Zn(neo)(nif)_2]$ (P = 0.9543). The A2780 model showed a significant decrease under treatment with cisPt (P = 0.0366, *), an insignificant increase with $[Zn(neo)(nif)_2]$ (P = 0.2785), and a significant difference between cisPt and $[Zn(neo)(nif)_2]$ (P = 0.0159, +). (**D**): The COX2/TGF-β1 protein expression ratio in HME1 showed an insignificant increase under treatment with cisPt (P = 0.4886) and an insignificant decrease with $[Zn(neo)(nif)_2]$ (P = 0.9328), as well as between cisPt and $[Zn(neo)(nif)_2]$ treatments (P = 0.5281). In 12Z cells, a significant increase was observed for control vs. cisPt (P < 0.0001, ***), an insignificant decrease for control vs. $[Zn(neo)(nif)_2]$ (P = 0.5485), and a significant difference between cisPt and $[Zn(neo)(nif)_2]$ (P < 0.0001, + + +). The A2780 model showed an insignificant increase under treatment with cisPt (P = 0.6724), a significant increase with $[Zn(neo)(nif)_2]$ (P = 0.0432, *), and significant difference between cisPt and $[Zn(neo)(nif)_2]$ (P = 0.0133, +). **E:** The VEGF-A/Nrf2 active protein expression ratio in HME1 showed an insignificant decrease under treatment with cisPt (P = 0.8258), a significant decrease with $[Zn(neo)(nif)_2]$ (P = 0.0254, *), and between cisPt and $[Zn(neo)(nif)_2]$ treatments (P = 0.0047, + +). In 12Z cells, a significant decrease was observed for control vs. cisPt (P = 0.0017, **), for control vs. $[Zn(neo)(nif)_2]$ (P = 0.0123, *), and between cisPt and $[Zn(neo)(nif)_2]$ (P = 0.0022, + +). The A2780 model showed an insignificant decrease under treatment with cisPt (P = 0.3470), a significant decrease wit $[Zn(neo)(nif)_2]$ (P = 0.0225, *), and a significant difference between cisPt and $[Zn(neo)(nif)_2]$ (P = 0.0240, +). **F:** The TGF-β1/Nrf2 active protein expression ratio in HME1 showed an insignificant decrease under treatment with cisPt (P = 0.9339) and $[Zn(neo)(nif)_2]$ (P = 0.8994), with no significant difference between cisPt and $[Zn(neo)(nif)_2]$ treatments (P = 0.9382). In 12Z cells, a significant decrease was observed for control vs. cisPt (P < 0.0001, ***), an insignificant decrease for control vs. $[Zn(neo)(nif)_2]$ (P = 0.2798), and a significant difference between cisPt and $[Zn(neo)(nif)_2]$ (P < 0.0001, + + +). The A2780 model showed a significant decrease under treatment with cisPt (P = 0.0097, **), an insignificant decrease with $[Zn(neo)(nif)_2]$ (P = 0.3477), and significant difference between cisPt and $[Zn(neo)(nif)_2]$ (P = 0.0016, + +).

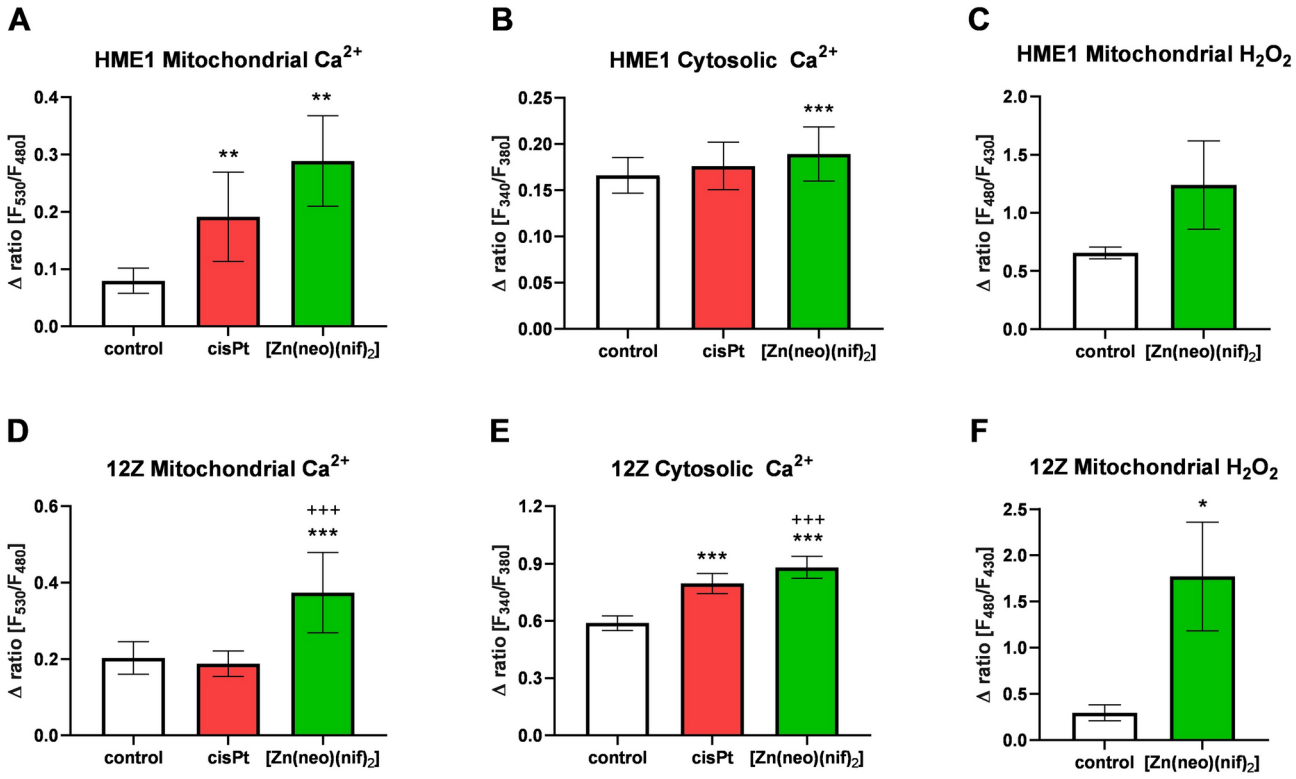

Fig. 7. (**A**, **D**): Mitochondrial Ca^{2+} levels under three tested conditions: control (untreated cells: HME1 n = 4; 12Z n = 14), cisPt (cells treated with 10 μM cis-platin: HME1 n = 6; 12Z n = 14), $[Zn(neo)(nif)_2]$ (cells treated with 10 μM $[Zn(neo)(nif)_2]$: HME1 n = 5; 12Z n = 14). (**B**, **E**): Cytosolic Ca^{2+} levels under three tested conditions: control (untreated cells: HME1 n = 46; 12Z n = 102), cisPt (cells treated with 10 μM cis-platin: HME1 n = 43; 12Z n = 88), $[Zn(neo)(nif)_2]$ (cells treated with 10 μM $[Zn(neo)(nif)_2]$: HME1 n = 50; 12Z n = 99). **C, F:** Mitochondrial H_2O_2 levels under two tested conditions: control (untreated cells: HME1 n = 3; 12Z n = 3), $[Zn(neo)(nif)_2]$ (cells treated with 10 μM $[Zn(neo)(nif)_2]$: HME1 n = 3; 12Z n = 4).

promotes angiogenesis[63]. The decreased VEGF-A/Nrf2 ratio (Fig. 6E) may indicate a potential reduction in angiogenic signals.

The role of ncRNA in cellular, tissue, and systemic metabolic processes is indisputable. MicroRNAs can exhibit both pro-angiogenic (miR-23a, -133b, let-7c) and anti-angiogenic (miR-206, -376a) effects. MicroRNAs known to influence VEGF-A expression, such as miR-206, negatively regulate angiogenesis by directly targeting VEGF-A[64]. Similarly, miR-23a reduces VEGF-A levels[65] but also downregulates Nrf2 and CAT, potentially altering ROS levels[66]. MiR-133b, which plays an oncogenic role in the progression of cervical carcinoma[67] and breast cancer[68], did not show significant changes in its ratio to VEGF-A expression (Fig. 4). The HME1 cell model showed a significant increase under treatment with cisPt, while no significant change was observed with $[Zn(neo)(nif)_2]$ treatment. In contrast, the 12Z and A2780 models exhibited a decrease in ratios, which was more pronounced and statistically significant in 12Z cells. Significant expression changes were observed in miR-206 in HME1 cells, miR-23a in 12Z cells, and miR-133b in HME1, 12Z, and A2780 cells (Figure S2). The anti-angiogenic miR-376a inhibits VEGF-A signaling by targeting SIRT1 or neuropilin 1 in various cancer cells[69].

In conclusion, we analyzed the let-7c/VEGF-A ratio (Fig. 4E) to further investigate the microRNA effect on VEGF-A expression. This pro-angiogenic microRNA showed a decreased ratio in all tested conditions in 12Z and A2780 cells. Chrishev et al. reported elevated expression of let-7c in ovarian tissue compared to endometrial tissue, suggesting that let-7c may have oncogenic effects with poor prognosis and lower overall survival[34], which aligns with our observations. The decreased let-7c expression observed in our tested conditions may indicate a better prognosis.

Since Ang1 stabilizes blood vessels while Ang2 induces angiogenesis, the elevated Ang2/Ang1 ratio (favoring Ang2) (Fig. 2A) likely reflects an active angiogenesis phase[70]. We hypothesize the observed increase in ANG2 expression alongside a simultaneous decrease in ANG1 under tested conditions may serve as an independent predictor of cell death, similar to findings reported by Ong et al.[71]. The ANG2/ANG1 ratio may be a valuable prognostic biomarker of endothelial activation in endometriosis or endometrioid adenocarcinoma, particularly in combination with altered expression of VEGF-A and TGF-β1[72].

Based on gene expression changes, we hypothesize that alterations in the Nrf2/COX2 ratio may reflect shifts in the regulatory roles of HIF-1α and COX2 in the Nrf2-mediated inflammatory response. The decreased CAS3/BAX ratio (Fig. 2E, 6B) suggests enhanced pro-apoptotic stimuli resulting from mitochondrial dysfunction closely linked to endoplasmic reticulum stress[73], potentially influenced by studied compounds in HME1 cells.

The observed elevation in the CAS3/BAX ratio in 12Z and A2780 under treatment with [Zn(neo)(nif)$_2$] may indicate the activation of CAS3 in programmed cell death processes[74].

MiR-206 has been reported to influence HIF-1α and Nrf2 expression in relation to ROS production and accumulation[75], as it inhibits cell growth even under high glucose metabolism conditions typical for cancer cells. We observed a decrease in the miR-206/HIF-1α ratio across all tested cell lines following cisPt treatment. In HME1 cells, treatment with [Zn(neo)(nif)$_2$] resulted in a significant increase in the miR-206/HIF-1α ratio, whereas a decrease was observed in 12Z and A2780 cells. This decrease may indicate increased resistance to apoptosis and could be indicative of disease progression[76].

The miR-206/Nrf2 ratio suggests upregulation of Nrf2 across all tested conditions, which may enhance antioxidant defense, cytoprotection, and resistance to oxidative stress-induced apoptosis. Conversely, a decrease in the miR-206/Nrf2 ratio may indicate the promotion of tumor progression, as Nrf2 can support cancer cell survival under stressful conditions. On the other hand, in oxidative disorders, a lower miR-206/Nrf2 ratio may protect by reducing oxidative damage[77] (Fig. 5C).

Nrf2 is a crucial regulator of endothelial miR-206-attenuated expression and can drive tumorigenesis through dysregulation of the Krebs cycle or pentose phosphate pathway[78]. The NRF2 pathway exhibits dual roles; it can act as a tumor suppressor by reducing ROS levels through its antioxidant function[79], yet it can also promote tumorigenesis by inducing ROS production and enhancing tumor growth[80]. The precise role of Nrf2 in the studied epithelial cell lines treated with tested compounds requires further investigation.

The findings suggest that the studied [Zn(neo)(if)$_2$] complex may contribute to mitochondrial calcium overload, resulting in increased ROS production. This mitochondrial Ca^{2+} accumulation could be associated with the activation of apoptotic genes (BAX, CAS3) and potential involvement of the mitochondrial permeability transition pore (mPTP). Furthermore, Ca^{2+} transfer through the mPTP may lead to elevated Ca^{2+} levels, which, together with increased ROS levels, could play a role in the induction of apoptosis or apoptosis-like cell death[81,82].

Material and methods

DNA binding studies

The double-stranded oligonucleotides ZnF3-7 (5'-TAGCGCCCCCTGCTGGC-3'/3'-ATCGCGGGGGACGACCG-5') and EBP (5'-ATTGCGCAAT-3'/3'-TAACGCGTTA-5') were prepared by annealing forward and reverse single-stranded oligonucleotide sequences, which were obtained from commercial suppliers (Sigma Aldrich).

Competitive fluorescence binding studies were conducted following a conventional procedure. Ethidium bromide (2,5 μM) was added to the respective oligonucleotides to form the DNA-EB complex. The studied compound was gradually added to this mixture at 0 to 5 μM concentrations.

The fluorescence emission spectra (λ_{EX} = 520 nm) were recorded after each addition of the complex, and the maximum emission intensity values were used to calculate the binding constants (K_{SV}) using the standard Stern–Volmer equation: $\frac{F_0}{F} = 1 + K_{SV}[Q]$.

Cell lines and cultivation protocol

We conducted experiments on three epithelial cell lines: HME1, 12Z, and A2780. The HME1 cell line (ExPASy htTERT-HME1) is an hTERT-immortalized cell line with epithelial morphology, derived from the breasts of a 53-year-old female patient undergoing reduction mammoplasty with no history of breast cancer. HME1 cells were used as a model of physiological angiogenesis. The 12Z cell line (a kind donation from Prof. Anna Starzinski-Powitz, Goethe-Universität Frankfurt) is an SV40 virus-immortalized cell line obtained from a 37-year-old female patient undergoing laparoscopy. This cell line exhibits expression of markers characteristic of endometriotic lesions observed in vivo. The A2780 cell line (a kind donation from Dr. Martina Šemeláková PhD., Pavol Jozef Šafárik University in Košice) is a human ovarian cancer cell line, originally established from an endometrioid adenocarcinoma of an untreated patient. The cell cultures were maintained to cell-specific protocols using appropriate culture media: Roswell Park Memorial Institute (RPMI) 1640 Medium for A2780 cells, Dulbecco's Modified Eagle's Medium (DMEM) for 12Z cells, Human Mammary Epithelial Cell Growth Medium (MEBM) mixed with Nutrient mixture medium F-12 Ham (1:1) for HME1 cells. All culture media were supplemented with 10% Fetal Bovine Serum (FBS) and 1% Penicillin/Streptomycin. The cells were incubated at 37°C in a humidified atmosphere containing 5% CO_2.

Cell transfection and treatment with tested compounds

All microscopic experiments were performed on 30 mm glass coverslips plated with cells in 6-well plates. Cells were transfected at 50–60% confluency with organelle-targeted biosensors: mitoHyPer7 (1.5 μg/well), mtD1GoCam (1.5 μg/well), the FRET-based Ca^{2+} biosensor 4mtD3cpv (1.5 μg/well), and cytosolic Ca^{2+} indicator Fura-2 acetoxy-methyl-ester (Fura-2AM) (1.5 μg/well), using 3 μL of TransFast transfection reagent (Promega, Madison, WI, USA) in 1 mL of serum and antibiotic-free medium for 8–12 h. Following transfection, the medium was replaced with 2 mL of experimental EH-loading buffer (Table S4), and measurements were conducted for 2–3 h at room temperature.

The tested compounds, cis-platin (cisPt) and [Zn(neo)(nif)$_2$], were used at a final concentration of 10 μM (based on IC_{50} – Table S5) in the appropriate complete cultivation medium. The compounds were applied to adherent cells (at the confluence 50–60%) or spheroid cells for 8 h, based on the results of the Cell Viability Assay (Figure S3).

3D tissue models

Our experiments utilized 3D tissue spheroids to study mRNA/miRNA expression, providing a more reliable tissue model for angiogenesis compared to the conventional 2D monolayer in vitro experiments. To form the spheroids, we used U-bottom 96 well-plates, with their surface coated with 0.8% LE agarose to create a thin

film non-adhesive film. Cells were seeded as a single-cell suspension (5—120 × 10^4 cells/mL, depending on the doubling time of each experimental tissue culture) in 200 µL of complete medium per well in the microtitration plates. The morphology of the spheroids for all experimental cell lines and in the tested conditions is shown in Figure S4.

Total RNA was extracted from the cell suspension using the RNeasy Mini Kit (Qiagen; Hilden, Germany) with a modified manufacturer's protocol. The isolated nucleic acid was transcribed into cDNA using the ProtoScript First Strand cDNA Synthesis Kit (New England Biolabs; Ipswich, MA, United States) and a thermocycler (Techne TC-3000X). qRT-PCR amplification was performed using SensiMIX II (Bioline Meridian Bioscience; London, England) on the Rotor-Gene Q system (Qiagen; Hilden, Germany) to detect the target mRNA expression.

For micro-RNA analysis, the isolated miRNA was processed using the TaqMan™ MicroRNA Reverse Transcription Kit (Applied Biosystems™) with the Techne TC-3000X thermocycler, followed by qRT-PCR amplification using the TaqMan™ Universal Master Mix II no UNG (Applied Biosystems™) on the thermocycler Rotor-Gene Q System (Qiagen; Hilden, Germany) to detect the target miRNA expression. The primer sequences and TaqMan probes used are listed in supplementary data (Table S6).

The obtained data were analyzed using Rotor-Gene Q 2.5.3 Software (Qiagen; Hilden, Germany), with relative mRNA expression normalized to the housekeeping gene β-Actin, and relative miRNA expression normalized to Ct40, as described by Gevaert et al.[83].

ELISA

The VEGF-A protein level was analyzed using the Human VEGF ELISA Kit (AB100662), while the TGF-β1 protein level was determined with the Human TGF beta 1 ELISA Kit (AB100647). The COX2 protein level was assessed using the Human COX2 ELISA Kit (AB267646), and the Nrf2 transcription factor was analyzed using the Human Nrf2 ELISA Kit (AB277397). The phosphorylated Nrf2 transcription factor was determined with the Nrf2 Transcription Factor Assay Kit (AB207223). All analyses were conducted on cell suspensions and followed the manufacturer's instructions (Abcam, Cambridge, UK).

ELISA plates were read at 450 nm using the SYNERGY HTX multi-mode reader (BioTek Instruments, Winooski, Vermont, USA), and data analysis was performed using Gen5 3.10 Software (BioTek Instruments). Quantification of the prepared samples was carried out using standard curve analysis.

Live-Cell Imaging

We conducted live-cell imaging experiments using the following equipment:

- A Zeiss array confocal laser scanning microscope (Axio Observer.Z1 from Zeiss, Gottingen, Germany) equipped with a 100 × objective lens (Plan-Fluor × 100/1.45 Oil, Zeiss, Germany), a motorized filter wheel (CSUX1FW, Yokogawa Electric Corporation, Tokyo, Japan) on the emission side, and an AOTF-based laser merge module for the 405, 445, 473, 488, 514, and 561 nm laser lines (Visitron Systems). The system included a Nipkow-based confocal scanning unit (CSU-X1, Yokogawa Electric Corporation). Data acquisition and fluorescence microscope control were performed using Visiview 4.2.01 (Visitron, Puchheim, Germany)[84].
- An inverted wide-field microscope Anglerfish (Observer.A1, Carl Zeiss GmbH, Vienna, Austria) with a 40 × oil immersion objective (Plan Apochromat 1,3 NA Oil DIC (UV) VISIR, Carl Zeiss GmbH, Vienna, Austria) and a standard CFP/YFP filter cube. Emission collection was facilitated by a 505dcxr beam-splitter, directing light to both sides of the camera (CCD camera, Coolsnap Dyno, Photometrics, Tucson, AZ, USA). Visualization was carried out using the NGFI AnglerFish C-Y7G imager for emission collected with Anglerfish.

A constant buffer perfusion flow was maintained using the NGFI perfusion system (PS9D, NGFI, Graz, Austria).

Mitochondrial H_2O_2 measurements

We measured mitochondrial H_2O_2 levels using the genetically encoded H_2O_2 sensors mitoHyper7. The mitoHyPer7 signals were imaged by alternately exciting the cells with a motorized dual filter system equipped with LED 480nm (excitation filter 480nm/17nm) and LED 430nm (excitation filter 433nm/24nm) beam splitters. Emissions were alternately collected using[78] a 535/22 BrightLine HC emission filter, as previously described by Tawfik et al.[85].

Cells were initially perfused with HEPES (4-(2-hydroxyethyl)-1-piperazineethanesulfonic acid) to record H_2O_2 production for the first 2 min. Subsequently, [Zn(neo)$(nif)_2$] (10 µM) was added for the following 6 min, and finally, cells were perfused again with HEPES for an additional 2 min.

The acquired data were saved as image files during the experiments and analyzed using Fiji software (ImageJ2). Background and photobleaching corrections were performed in Excel, and data were analyzed further using GraphPad Prism 8.01.

Cytosolic Ca^{2+} measurements

We measured cytosolic Ca^{2+} concentrations in cells incubated with the fluorescent cytosolic Ca^{2+} indicator Fura-2 acetoxy-methyl-ester (Fura-2AM) (TEFLabs, Austin, TX) for 30 min in EH-loading buffer. Cells stained with Fura-2AM were illuminated at 340 nm and 380 nm, with emission captured at 515 nm, as previously described[86]. The measurements were recorded as the F380/F340 ratio using live-acquisition software v2.0.0.12 (Till Photonics) and analyzed using GraphPad Prism 8.01. Background subtraction was performed using a designated background region of interest (ROI), and bleaching correction was applied using an exponential decay fit of the basal fluorescence extrapolated across the entire measurement. The results represent the maximal (Δmax) in cytosolic Ca^{2+} levels in response to ATP or histamine (100 µmol/L) stimulation of the cells.

Mitochondrial Ca^{2+} measurements

Mitochondrial Ca^{2+} measurements were conducted using the genetically encoded biosensor 4mtD3cpv. The excitation wavelength for 4mtD3cpv was set at 440 nm (440AF21, Omega Optical, Brattleboro, VT, USA), and emissions were captured at 480 and 535 nm (480AF30 and 535AF26, Omega Optical, Brattleboro, VT, USA) as previously described[86]. Data acquisition was performed using NIS-Elements AR software (Nikon, Vienna, Austria) and analyzed using GraphPad Prism 8.01. Measurements were corrected by a background region of interest (ROI), and photobleaching correction was applied using an exponential decay fit. The results represent the maximal change (Δmax) in mitochondrial Ca^{2+} levels in response to ATP or histamine (100 µmol/L) stimulation of the cells.

Statistical analysis

The experimental qRT-PCR mRNA data were analyzed using GraphPad Prism 8.01 (GraphPad Software, San Diego, CA, USA) and are represented as mean values ± SD of three independent measurements provided in duplicate (one independent measurement was provided in duplicate for miRNA determination and one independent measurement was provided in triplicate for GPx1 and SOD1, respectively).

Cytosolic calcium measurement data were evaluated using GraphPad Prism 8.01 and are expressed as mean values ± SD of three independent measurements for untreated cells: HME1 (n = 46) and 12Z (n = 102); cells treated with 10 µM cis-platin: HME1 (n = 43) and 12Z (n = 88); and cells treated with 10 µM $[Zn(neo)(nif)_2]$: HME1 (n = 50) and 12Z (n = 99).

Mitochondrial calcium measurement data were analyzed using GraphPad Prism 8.01 and are represented as mean values ± SD of three independent measurements for untreated cells: HME1 (n = 4) and 12Z (n = 14); cells treated with 10 µM cis-platin: HME1 (n = 6) and 12Z (n = 14); and cells treated with 10 µM $[Zn(neo)(nif)_2]$) HME1 (n = 5) and 12Z (n = 14).

Mitochondrial H_2O_2 data were analyzed using GraphPad Prism 8.01 and are represented as mean values ± SD of three independent measurements for untreated cells: HME1 (n = 3) and 12Z (n = 3); and cells treated with 10 µM $[Zn(neo)(nif)_2]$: HME1 (n = 3) and 12Z (n = 4).

Statistical analysis was performed using the Student's t-test and nonparametric analysis of variance (ANOVA), followed by Tukey's post hoc test and Dunnett 's Multiple Comparison test. Statistically significant results were found as follows: P-value < 0.05 (*, significant), P-value < 0.01 (**, highly significant), and P-value < 0.001 (***, strongly significant).

Data availability

The datasets used and/or analyzed during the current study are available from the corresponding author upon reasonable request.

Received: 11 June 2024; Accepted: 12 March 2025
Published online: 24 March 2025

References

1. Huang, M., Chen, Y., Han, D., Lei, Z. & Chu, X. Role of the zinc finger and SCAN domain-containing transcription factors in cancer. *Am. J. Cancer Res.* **9**, 816–836 (2019).
2. Nguyen, T., Nioi, P. & Pickett, C. B. The Nrf2-Antioxidant Response Element Signaling Pathway and Its Activation by Oxidative Stress. *J. Biol. Chem.* **284**, 13291–13295 (2009).
3. Tang, Y. et al. MicroRNAs and angiogenesis: a new era for the management of colorectal cancer. *Cancer Cell Int.* **21**, 221 (2021).
4. Zhao, Y., Xing, C., Deng, Y., Ye, C. & Peng, H. HIF-1α signaling: Essential roles in tumorigenesis and implications in targeted therapies. *Genes Dis.* **11**, 234–251 (2024).
5. Rytkönen, K. T. et al. Histone H3K4me3 breadth in hypoxia reveals endometrial core functions and stress adaptation linked to endometriosis. *Iscience* **25**, 104235 (2022).
6. Zhu, H. & Zhang, S. Hypoxia inducible factor-1α/vascular endothelial growth factor signaling activation correlates with response to radiotherapy and its inhibition reduces hypoxia-induced angiogenesis in lung cancer. *J. Cell. Biochem.* **119**, 7707–7718 (2018).
7. deSouza, N. M., Choudhury, A., Greaves, M., O'Connor, J. P. B. & Hoskin, P. J. Imaging hypoxia in endometrial cancer: How and why should it be done?. *Front. Oncol.* **12**, 1020907 (2022).
8. Huang, Y.-J. & Nan, G.-X. Oxidative stress-induced angiogenesis. *J. Clin. Neurosci.* **63**, 13–16 (2019).
9. Lugano, R., Ramachandran, M. & Dimberg, A. Tumor angiogenesis: causes, consequences, challenges and opportunities. *Cell. Mol. Life Sci.* **77**, 1745–1770 (2020).
10. Lan, J., Huang, Z., Han, J., Shao, J. & Huang, C. Redox regulation of microRNAs in cancer. *Cancer Lett.* **418**, 250–259 (2018).
11. Hua, Y.-T., Xu, W.-X., Li, H. & Xia, M. Emerging roles of MiR-133a in human cancers. *J. Cancer* **12**, 198–206 (2021).
12. Li, Y. et al. MEG3 sponges miRNA-376a and YBX1 to regulate angiogenesis in ovarian cancer endothelial cells. *Heliyon* **9**, e13204 (2023).
13. Tian, X. et al. Exosome-derived miR-let-7c promotes angiogenesis in multiple myeloma by polarizing M2 macrophages in the bone marrow microenvironment. *Leuk. Res.* **105**, 106566 (2021).
14. Huang, S. et al. MicroRNA-181a modulates gene expression of zinc finger family members by directly targeting their coding regions. *Nucleic Acids Res.* **38**, 7211–7218 (2010).
15. Deeksha, W., Abhishek, S. & Rajakumara, E. PAR recognition by PARP1 regulates DNA-dependent activities and independently stimulates catalytic activity of PARP1. *FEBS J.* **290**, 5098–5113 (2023).
16. Wei, W., Li, Y., Lv, S., Zhang, C. & Tian, Y. PARP-1 may be involved in angiogenesis in epithelial ovarian cancer. *Oncol. Lett.* **12**, 4561–4567 (2016).
17. Peng, X. et al. Selective PARP1 inhibitors, PARP1-based dual-target inhibitors, PROTAC PARP1 degraders, and prodrugs of PARP1 inhibitors for cancer therapy. *Pharmacol. Res.* **186**, 106529 (2022).
18. Munoz, F. M., Zhang, F., Islas-Robles, A., Lau, S. S. & Monks, T. J. From the Cover: ROS-Induced Store-Operated Ca2+ Entry Coupled to PARP-1 Hyperactivation Is Independent of PARG Activity in Necrotic Cell Death. *Toxicol. Sci.* **158**, 444–453 (2017).
19. Ahmed, S. M. U., Luo, L., Namani, A., Wang, X. J. & Tang, X. Nrf2 signaling pathway: Pivotal roles in inflammation. *Biochim. Biophys. Acta BBA Mol. Basis Dis.* **1863**, 585–597 (2017).

20. Granatiero, V., Konrad, C., Bredvik, K., Manfredi, G. & Kawamata, H. Nrf2 signaling links ER oxidative protein folding and calcium homeostasis in health and disease. *Life Sci. Alliance* **2**, e201900563 (2019).
21. Kobayashi, H., Kimura, M., Maruyama, S., Nagayasu, M. & Imanaka, S. Revisiting estrogen-dependent signaling pathways in endometriosis: Potential targets for non-hormonal therapeutics. *Eur. J. Obstet. Gynecol. Reprod. Biol.* **258**, 103–110 (2021).
22. Chen, C.-H. Defense Against Oxidative Stress: Nrf2-ARE Pathway. in *Activation and Detoxification Enzymes* 151–160 (Springer Nature Switzerland, Cham, 2024). https://doi.org/10.1007/978-3-031-55287-8_13.
23. Devlieger, R. et al. Maternal obesity in Europe: where do we stand and how to move forward?. *Eur. J. Obstet. Gynecol. Reprod. Biol.* **201**, 203–208 (2016).
24. Hsu, W.-L. et al. Blockage of Nrf2 and autophagy by L-selenocystine induces selective death in Nrf2-addicted colorectal cancer cells through p62-Keap-1-Nrf2 axis. *Cell Death Dis.* **13**, 1060 (2022).
25. Harel, S., Sanchez-Gonzalez, V., Echavarria, R., Mayaki, D. & Hussain, S. N. Roles of miR-640 and Zinc Finger Protein 91 (ZFP91) in Angiopoietin-1-Induced In Vitro Angiogenesis. *Cells* **9**, 1602 (2020).
26. Wang, L. et al. Nrf2 Activation Enhances Muscular MCT1 Expression and Hypoxic Exercise Capacity. *Med. Sci. Sports Exerc.* **52**, 1719–1728 (2020).
27. Tachibana, I. et al. Overexpression of the TGFbeta-regulated zinc finger encoding gene, TIEG, induces apoptosis in pancreatic epithelial cells. *J. Clin. Invest.* **99**, 2365–2374 (1997).
28. Liu, S., Liu, X., Lin, X. & Chen, H. Zinc Finger Proteins in the War on Gastric Cancer: Molecular Mechanism and Clinical Potential. *Cells* **12**, 1314 (2023).
29. Gołąbek-Grenda, A. & Olejnik, A. In vitro modeling of endometriosis and endometriotic microenvironment – Challenges and recent advances. *Cell. Signal.* **97**, 110375 (2022).
30. Nathan, J., Shameera, R. & Palanivel, G. Studying molecular signaling in major angiogenic diseases. *Mol. Cell. Biochem.* **477**, 2433–2450 (2022).
31. Roškar, L., Roškar, I., Rižner, T. L. & Smrkolj, Š. Diagnostic and Therapeutic Values of Angiogenic Factors in Endometrial Cancer. *Biomolecules* **12**, 7 (2021).
32. Clower, L., Fleshman, T., Geldenhuys, W. J. & Santanam, N. Targeting Oxidative Stress Involved in Endometriosis and Its Pain. *Biomolecules* **12**, 1055 (2022).
33. Rabajdová, M. et al. Zinc(II) niflumato complex effects on MMP activity and gene expression in human endometrial cell lines. *Sci. Rep.* **11**, 19086 (2021).
34. Chirshev, E., Oberg, K. C., Ioffe, Y. J. & Unternaehrer, J. J. *Let - 7* as biomarker, prognostic indicator, and therapy for precision medicine in cancer. *Clin. Transl. Med.* **8**, e24 (2019).
35. Liu, T., Lv, Y.-F., Zhao, J.-L., You, Q.-D. & Jiang, Z.-Y. Regulation of Nrf2 by phosphorylation: Consequences for biological function and therapeutic implications. *Free Radic. Biol. Med.* **168**, 129–141 (2021).
36. Bhat, S. et al. ZNF471 modulates EMT and functions as methylation regulated tumor suppressor with diagnostic and prognostic significance in cervical cancer. *Cell Biol. Toxicol.* **37**, 731–749 (2021).
37. Eelen, G., Treps, L., Li, X. & Carmeliet, P. Basic and Therapeutic Aspects of Angiogenesis Updated. *Circ. Res.* **127**, 310–329 (2020).
38. Xu, X.-W. et al. A narrative review of research progress on the relationship between hypoxia-inducible factor-2α and wound angiogenesis. *Ann. Palliat. Med.* **10**, 4882–4888 (2021).
39. Lamceva, J., Uljanovs, R. & Strumfa, I. The Main Theories on the Pathogenesis of Endometriosis. *Int. J. Mol. Sci.* **24**, 4254 (2023).
40. Larabee, J. L., Hocker, J. R. & Hanas, J. S. Mechanisms of inhibition of zinc-finger transcription factors by selenium compounds ebselen and selenite. *J. Inorg. Biochem.* **103**, 419–426 (2009).
41. Kuramoto, K. et al. ZK7, a novel zinc finger gene, is induced by vascular endothelial growth factor and inhibits apoptotic death in hematopoietic cells. *Cancer Res.* **60**, 425–430 (2000).
42. Zhao, J., Wen, D., Zhang, S., Jiang, H. & Di, X. The role of zinc finger proteins in malignant tumors. *FASEB J.* **37**, e23157 (2023).
43. Duran, C. L. et al. Targeting Tie2 in the Tumor Microenvironment: From Angiogenesis to Dissemination. *Cancers* **13**, 5730 (2021).
44. Wang, Q. & Lash, G. E. Angiopoietin 2 in placentation and tumor biology: The yin and yang of vascular biology. *Placenta* **56**, 73–78 (2017).
45. Du, L. et al. ZNF3 regulates proliferation, migration and invasion through MMP1 and TWIST in colorectal cancer. *Acta Biochim. Biophys. Sin.* https://doi.org/10.3724/abbs.2022187 (2022).
46. Pages, B. J., Ang, D. L., Wright, E. P. & Aldrich-Wright, J. R. Metal complex interactions with DNA. *Dalton Trans.* **44**, 3505–3526 (2015).
47. Maganti, L. & Bhattacharyya, D. Sequence specificity in DNA–drug intercalation: MD simulation and density functional theory approaches. *J. Comput. Aided Mol. Des.* **34**, 83–95 (2020).
48. Smolko, L. et al. Zinc(II) niflumato complex with neocuproine: Synthesis, crystal structure, characterization and cytotoxic effects on human endometrial cell lines. *J. Mol. Struct.* **1237**, 130312 (2021).
49 Pavletich, N. P. & Pabo, C. O. Zinc Finger-DNA Recognition: Crystal Structure of a Zif268-DNA Complex at 2.1 Å. *Science* **252**, 809–817 (1991).
50. Hashimoto, H. et al. Structural Basis for the Versatile and Methylation-Dependent Binding of CTCF to DNA. *Mol. Cell* **66**, 711-720.e3 (2017).
51. Spender, L. C. et al. TGF-β induces apoptosis in human B cells by transcriptional regulation of BIK and BCL-XL. *Cell Death Differ.* **16**, 593–602 (2009).
52. Tang, Z., Ow, G. S., Thiery, J. P., Ivshina, A. V. & Kuznetsov, V. A. Meta-analysis of transcriptome reveals let-7b as an unfavorable prognostic biomarker and predicts molecular and clinical subclasses in high-grade serous ovarian carcinoma. *Int. J. Cancer* **134**, 306–318 (2014).
53. Ferrari, G., Cook, B. D., Terushkin, V., Pintucci, G. & Mignatti, P. Transforming growth factor-beta 1 (TGF-β1) induces angiogenesis through vascular endothelial growth factor (VEGF)-mediated apoptosis. *J. Cell. Physiol.* **219**, 449–458 (2009).
54. Dhahri, W. et al. Reduced expression of let-7f activates TGF -β/ ALK 5 pathway and leads to impaired ischaemia-induced neovascularization after cigarette smoke exposure. *J. Cell. Mol. Med.* **21**, 2211–2222 (2017).
55. Huang, S. et al. Transcriptional downregulation of miR-133b by REST promotes prostate cancer metastasis to bone via activating TGF-β signaling. *Cell Death Dis.* **9**, 779 (2018).
56. Pickup, M., Novitskiy, S. & Moses, H. L. The roles of TGFβ in the tumour microenvironment. *Nat. Rev. Cancer* **13**, 788–799 (2013).
57 Fong, C. Y., Pang, L., Holland, E. & Knox, A. J. TGF-β1 stimulates IL-8 release, COX-2 expression, and PGE_2 release in human airway smooth muscle cells. *Am. J. Physiol. Lung Cell. Mol. Physiol.* https://doi.org/10.1152/ajplung.2000.279.1.L201 (2000).
58. Churchman, A. T. et al. Transforming growth factor-β_1 elicits Nrf2-mediated antioxidant responses in aortic smooth muscle cells. *J. Cell. Mol. Med.* **13**, 2282–2292 (2009).
59. Genrich, G. et al. The anti-oxidative transcription factor Nuclear factor E2 related factor-2 (Nrf2) counteracts TGF-β1 mediated growth inhibition of pancreatic ductal epithelial cells -Nrf2 as determinant of pro-tumorigenic functions of TGF-β1. *BMC Cancer* **16**, 155 (2016).
60. Bu, M. T., Chandrasekhar, P., Ding, L. & Hugo, W. The roles of TGF-β and VEGF pathways in the suppression of antitumor immunity in melanoma and other solid tumors. *Pharmacol. Ther.* **240**, 108211 (2022).
61. Geng, L., Chaudhuri, A., Talmon, G., Wisecarver, J. L. & Wang, J. TGF-Beta Suppresses VEGFA-Mediated Angiogenesis in Colon Cancer Metastasis. *PLoS ONE* **8**, e59918 (2013).

62. Young, V. J., Ahmad, S. F., Brown, J. K., Duncan, W. C. & Horne, A. W. Peritoneal VEGF-A expression is regulated by TGF-β1 through an ID1 pathway in women with endometriosis. *Sci. Rep.* **5**, 16859 (2015).
63. Kweider, N. et al. Interplay between Vascular Endothelial Growth Factor (VEGF) and Nuclear Factor Erythroid 2-related Factor-2 (Nrf2). *J. Biol. Chem.* **286**, 42863–42872 (2011).
64. Cai, Y., Li, H. & Zhang, Y. Downregulation of microRNA-206 suppresses clear cell renal carcinoma proliferation and invasion by targeting vascular endothelial growth factor A. *Oncol. Rep.* **35**, 1778–1786 (2016).
65. Sun, L., Liu, X. & Zuo, Z. Regulatory role of miRNA-23a in diabetic retinopathy. *Exp. Ther. Med.* **22**, 1477 (2021).
66. Li, L. X. et al. MiR-23a-5p exacerbates intestinal ischemia–reperfusion injury by promoting oxidative stress via targeting PPAR alpha. *Biochem. Pharmacol.* **180**, 114194 (2020).
67. Qin, W. et al. MicroRNA-133b is a key promoter of cervical carcinoma development through the activation of the ERK and AKT1 pathways. *Oncogene* **31**, 4067–4075 (2012).
68. Wang, Q.-Y. et al. MiR-133b targets Sox9 to control pathogenesis and metastasis of breast cancer. *Cell Death Dis.* **9**, 752 (2018).
69. Deng, Y.-W., Shu, Y.-G. & Sun, S.-L. miR-376a inhibits glioma proliferation and angiogenesis by regulating YAP1/VEGF signalling via targeting of SIRT1. *Transl. Oncol.* **15**, 101270 (2022).
70. Senna, M. K., Machaly, S. A., Foda, M. & Eid, N. Baseline angiopoietin-2/angiopoietin-1 (Ang2/Ang1) ratio is correlated with the synovial vascularity measured 1 month later in rheumatoid arthritis. *Egypt. Rheumatol. Rehabil.* **40**, 193–197 (2013).
71. Ong, T. et al. Ratio of angiopoietin-2 to angiopoietin-1 as a predictor of mortality in acute lung injury patients: *Crit. Care Med.* **38**, 1845–1851 (2010).
72. Abdulkadir, S. et al. Modulating Angiogenesis by Proteomimetics of Vascular Endothelial Growth Factor. *J. Am. Chem. Soc.* **144**, 270–281 (2022).
73. Liu, Y. et al. Mitochondria-associated endoplasmic reticulum membrane (MAM): a dark horse for diabetic cardiomyopathy treatment. *Cell Death Discov.* **10**, 148 (2024).
74. Peña-Blanco, A. & García-Sáez, A. J. Bax, Bak and beyond — mitochondrial performance in apoptosis. *FEBS J.* **285**, 416–431 (2018).
75. Bai, Z. et al. The Role of MicroRNA-206 in the Regulation of Diabetic Wound Healing via Hypoxia-Inducible Factor 1-Alpha. *Biochem. Genet.* https://doi.org/10.1007/s10528-024-10759-9 (2024).
76. Jiang, Q. et al. Circular RNA-ZNF532 regulates diabetes-induced retinal pericyte degeneration and vascular dysfunction. *J. Clin. Invest.* **130**, 3833–3847 (2020).
77. Pacheco, J. & Schenk, E. CDK4/6 inhibition alone and in combination for non-small cell lung cancer. *Oncotarget* **10**, 618–619 (2019).
78. Singh, A. et al. Transcription factor NRF2 regulates miR-1 and miR-206 to drive tumorigenesis. *J. Clin. Invest.* **123**, 2921–2934 (2013).
79. Occhiuto, C. J., Moerland, J. A., Leal, A. S., Gallo, K. A. & Liby, K. T. The Multi-Faceted Consequences of NRF2 Activation throughout Carcinogenesis. *Mol. Cells* **46**, 176–186 (2023).
80. DeNicola, G. M. et al. Oncogene-induced Nrf2 transcription promotes ROS detoxification and tumorigenesis. *Nature* **475**, 106–109 (2011).
81. Bauer, T. M. & Murphy, E. Role of Mitochondrial Calcium and the Permeability Transition Pore in Regulating Cell Death. *Circ. Res.* **126**, 280–293 (2020).
82. Görlach, A., Bertram, K., Hudecova, S. & Krizanova, O. Calcium and ROS: A mutual interplay. *Redox Biol.* **6**, 260–271 (2015).
83. Gevaert, A. B. et al. MicroRNA profiling in plasma samples using qPCR arrays: Recommendations for correct analysis and interpretation. *PLOS ONE* **13**, e0193173 (2018).
84. Madreiter-Sokolowski, C. T. et al. PRMT1-mediated methylation of MICU1 determines the UCP2/3 dependency of mitochondrial Ca2+ uptake in immortalized cells. *Nat. Commun.* **7**, 12897 (2016).
85. Tawfik, I. et al. T3-induced enhancement of mitochondrial Ca2+ uptake as a boost for mitochondrial metabolism. *Free Radic. Biol. Med.* **181**, 197–208 (2022).
86. Madreiter-Sokolowski, C. T., Gottschalk, B., Sokolowski, A. A., Malli, R. & Graier, W. F. Dynamic Control of Mitochondrial Ca2+ Levels as a Survival Strategy of Cancer Cells. *Front. Cell Dev. Biol.* **9**, 614668 (2021).

Author contributions

Conceptualization, I.Š. and M.R.; methodology, I.Š., and L.S.; validation, Z.B., K.K., and C.M.-S.; formal analysis, I.Š., L.S., Z.B., K.K.; investigation, I.Š.; resources, J.V.; data curation, I.Š. and L.S.; writing—original draft preparation, G.S., L.S., and I.Š.; writing—review and editing, L.S., J.V., C.M.-S., and M.R.; visualization, I.Š., and L.S.; supervision, M.R., W.F.G., and J.V.; project administration, M.R., M.M., and J.V.; funding acquisition, M.R. and W.F.G. All authors reviewed the manuscript.

Funding

This research was funded by Slovak Grant Agency VEGA 1/0435/23 and the Austrian Science Funds (FWF) [DOI: 10.55776/W1226].

Declarations

Competing interests

The authors declare no competing interests.

Additional information

Supplementary Information The online version contains supplementary material available at https://doi.org/10.1038/s41598-025-94249-x.

Correspondence and requests for materials should be addressed to M.R.